Article

Cell

Replication-Dependent Unhooking of DNA Interstrand Cross-Links by the NEIL3 Glycosylase

Graphical Abstract

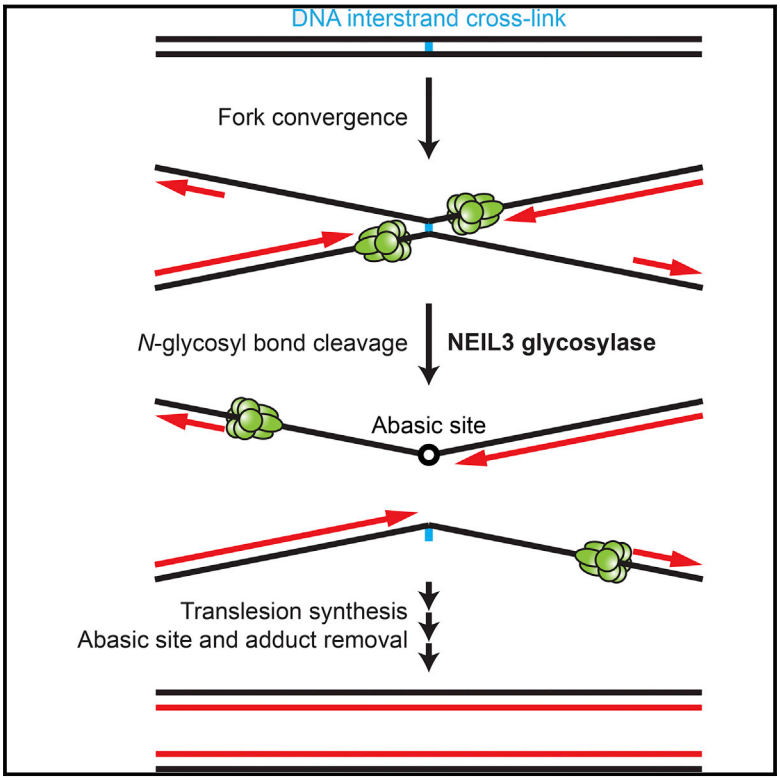

Highlights

- Distinct mechanisms resolve different DNA interstrand cross-links (ICLs)
- Psoralen and abasic site ICL repair is independent of DNA breaks and FANCI-FANCD2
- The NEIL3 DNA glycosylase resolves psoralen and abasic site ICLs
- FANCI-FANCD2-dependent ICL resolution predominates in the absence of NEIL3

Authors

Daniel R. Semlow, Jieqiong Zhang, Magda Budzowska, Alexander C. Drohat, Johannes C. Walter

Correspondence

johannes_walter@hms.harvard.edu

In Brief

Active deglycosylation drives a new incision-independent repair pathway responsible for resolving interstrand cross-links.

Semlow et al., 2016, Cell *167*, 1–14
October 6, 2016
http://dx.doi.org/10.1016/j.cell.2016.09.008

CellPress

Please cite this article in press as: Semlow et al., Replication-Dependent Unhooking of DNA Interstrand Cross-Links by the NEIL3 Glycosylase, Cell (2016), http://dx.doi.org/10.1016/j.cell.2016.09.008

Article

Cell

Replication-Dependent Unhooking of DNA Interstrand Cross-Links by the NEIL3 Glycosylase

Daniel R. Semlow,[1,4] Jieqiong Zhang,[1,4,5] Magda Budzowska,[1,6] Alexander C. Drohat,[2] and Johannes C. Walter[1,3,7,*]
[1]Department of Biological Chemistry and Molecular Pharmacology, Harvard Medical School, Boston, MA 02115, USA
[2]Department of Biochemistry and Molecular Biology, University of Maryland School of Medicine, Baltimore, MD 21201, USA
[3]Howard Hughes Medical Institute, Department of Biological Chemistry and Molecular Pharmacology, Harvard Medical School, Boston, MA 02115, USA
[4]Co-first author
[5]Present address: Department of Physiological Chemistry, Genentech Inc., South San Francisco, CA 94080, USA
[6]Present address: The NNF Center for Protein Research, Copenhagen University, Copenhagen 1017, Denmark
[7]Lead Contact
*Correspondence: johannes_walter@hms.harvard.edu
http://dx.doi.org/10.1016/j.cell.2016.09.008

SUMMARY

During eukaryotic DNA interstrand cross-link (ICL) repair, cross-links are resolved ("unhooked") by nucleolytic incisions surrounding the lesion. In vertebrates, ICL repair is triggered when replication forks collide with the lesion, leading to FANCI-FANCD2-dependent unhooking and formation of a double-strand break (DSB) intermediate. Using *Xenopus* egg extracts, we describe here a replication-coupled ICL repair pathway that does not require incisions or FANCI-FANCD2. Instead, the ICL is unhooked when one of the two *N*-glycosyl bonds forming the cross-link is cleaved by the DNA glycosylase NEIL3. Cleavage by NEIL3 is the primary unhooking mechanism for psoralen and abasic site ICLs. When *N*-glycosyl bond cleavage is prevented, unhooking occurs via FANCI-FANCD2-dependent incisions. In summary, we identify an incision-independent unhooking mechanism that avoids DSB formation and represents the preferred pathway of ICL repair in a vertebrate cell-free system.

INTRODUCTION

DNA replication and transcription require DNA unwinding. Therefore, chemical agents that create DNA interstrand cross-links (ICLs) are extremely cytotoxic. ICLs are induced by diverse chemical agents (Deans and West, 2009), including nitrogen mustards, platinum compounds, mitomycin C, and psoralen, which are used in chemotherapy. ICLs can also be generated by endogenous agents, most notably formaldehyde, acetaldehyde, and malondialdehyde (Duxin and Walter, 2015). In addition, the deoxyribose sugar of an abasic (AP) site (generated by spontaneous hydrolysis or the action of a DNA glycosylase) can isomerize to a ring-open aldehyde that is attacked by a base on the opposite strand, generating an "AP-ICL" (Price et al., 2014). Given that mammalian cells contain ~100,000 AP sites at steady state (Nakamura and Swenberg, 1999), AP-ICLs may form in vivo. ICLs are chemically and structurally diverse. Cisplatin links guanines on opposing strands through their N7 nitrogens. The resulting ICL is so distorting that the cytidines opposite the crosslinked guanosines are flipped out of the DNA helix. Upon exposure to UV light, psoralen links thymines on opposite strands, but the resulting ICL is not highly distorting. Reactive aldehydes generally induce cross-links between the exocyclic amines of bases, but little is known about their structure. An important question is whether these chemically diverse ICLs are repaired via similar or distinct strategies.

The vertebrate ICL repair pathway that contributes most to cell survival is coupled to DNA replication (Clauson et al., 2013; Kottemann and Smogorzewska, 2013; Zhang and Walter, 2014). This pathway involves structure-specific endonucleases, DNA recombinases, and translesion synthesis (TLS) polymerases. In addition, it requires 19 "FANC" proteins, mutations in which cause the bone marrow failure and cancer predisposition syndrome Fanconi anemia. A key factor in this pathway is the FANCI-FANCD2 heterodimer (FANCI-D2), whose mono-ubiquitylation protects cells from ICL-inducing agents. Importantly, the Fanconi pathway also protects cells from the genotoxic effects of endogenous aldehydes, though the nature of the relevant DNA lesions is presently unclear (Duxin and Walter, 2015; Garaycoechea et al., 2012; Langevin et al., 2011; Pontel et al., 2015).

By replicating a plasmid containing a site-specific cisplatin ICL in *Xenopus* egg extracts, we previously described a mechanism of replication-coupled ICL repair (Figure S1A; Räschle et al., 2008). The leading strands of converging replication forks initially stall ~20 nt from the lesion due to steric hindrance by the replicative CDC45/MCM2-7/GINS (CMG) helicase, which encircles and travels along the leading-strand template ahead of DNA polymerase (Fu et al., 2011). The first known event in repair is removal of the stalled CMGs, which requires fork convergence, the tumor suppressor BRCA1-BARD1, and ubiquitin signaling (Long et al., 2014; Zhang et al., 2015). Subsequently, the leading strand is extended to within 1 nt of the ICL ("−1" position). Ubiquitylated FANCI-D2 then binds near the ICL and helps recruit the XPF-ERCC1-SLX4 complex, which promotes incisions surrounding the ICL (Klein Douwel et al., 2014; Knipscheer et al., 2009). This "unhooking" reaction creates a double-stranded DNA break in one sister chromatid and a mono-adduct in the

other strand, which is bypassed with ~98% accuracy using the TLS polymerase REV1-Pol ζ (Budzowska et al., 2015). The DSB is repaired by RAD51-dependent homologous recombination (Long et al., 2011). The remaining mono-adduct is not removed in egg extracts, although this may occur in cells. A similar mechanism of repair was observed for a nitrogen-mustard-like-ICL (Räschle et al., 2008). Because this cell-free system requires all the major proteins implicated in ICL repair in cells, it likely recapitulates physiological repair. Importantly, all eukaryotic mechanisms of ICL repair described so far, including those operating outside of S phase (Williams et al., 2013), involve nucleolytic incisions to unhook the cross-link.

We wanted to address whether chemically diverse ICLs are repaired by similar or different mechanisms in *Xenopus* egg extracts. We therefore prepared plasmids containing a psoralen- or AP-ICL and incubated them in egg extract alongside a cisplatin-ICL plasmid. Strikingly, although repair of psoralen- and AP-ICLs requires replication fork convergence, as seen for the cisplatin-ICL, the downstream repair events are completely different. Specifically, one of the two *N*-glycosyl bonds that form the psoralen- or AP-ICL is cleaved by the NEIL3 DNA glycosylase, unhooking the cross-link in the absence of incisions. This reaction does not require FANCI-D2 or CMG unloading. After unhooking, gaps are filled in via TLS polymerases. When *N*-glycosyl bond cleavage is inhibited, repair switches to FANCI-D2-dependent incisions. Thus, *N*-glycosyl cleavage by NEIL3 represents the primary unhooking pathway for psoralen- and AP-ICLs, whereas incisions represent a backup mechanism. We conclude that ICLs can be unhooked via two independent mechanisms in S phase, one of which avoids DSB formation and thus minimizes the potential for gross chromosomal rearrangements.

RESULTS

pICL^{Pso} Repair in the Absence of DSB Formation

To examine the mechanism of psoralen-ICL repair, we prepared a 5.6-kb plasmid containing a site-specific psoralen-ICL (Figures 1A and S1B; pICL^{Pso}) and replicated it in *Xenopus* egg extracts containing [α-^{32}P]dATP alongside undamaged (pCtrl) and cisplatin-ICL-containing plasmids (Figure 1A; pICL^{Pt}). Replication intermediates were examined by native gel electrophoresis and autoradiography. pCtrl was rapidly converted to open circular and supercoiled replication products (Figure 1C, lanes 1–10). In contrast, on pICL^{Pt} and pICL^{Pso}, replication forks converged on the ICL, leading to the accumulation of "figure 8" structures (Figures 1C, 1Bi, and 1Di; Räschle et al., 2008). During pICL^{Pt} repair, dual incisions of the figure 8 intermediate generated a DSB that is repaired via HR with the other sister (Figure 1Biii; Long et al., 2011). The resulting HR intermediates were detected near the top of the gel (Figure 1C, arrowhead; Long et al., 2011). Concurrently, supercoiled (SC) molecules accumulated (Figure 1C, lanes 15–20). Surprisingly, during pICL^{Pso} repair, HR intermediates were scarce, and figure 8 structures appeared to be directly converted into open circular molecules (nicked or gapped; OC) and then supercoiled species (Figure 1C, lanes 21–30). As seen for pICL^{Pt} (Räschle et al., 2008), unhooking and error-free repair of pICL^{Pso} was replication dependent (Figures S1C–S1F), although the efficiency of repair was low (Figure S1G; see Discussion). Furthermore, when only a single fork encountered the psoralen-ICL, it failed to trigger ICL processing (Zhang et al., 2015). The data above indicate that psoralen-ICL repair, although dependent on replication fork convergence, might involve a novel mechanism.

Given the apparent absence of HR products during pICL^{Pso} repair, we examined whether this process involves a DSB intermediate. During pICL^{Pt} repair, FANCI-D2-promotes incisions around the ICL (Figures 1Bi and 1Bii; Klein Douwel et al., 2014; Knipscheer et al., 2009; Räschle et al., 2008) that are detected as 3.6-kb and 2.0-kb fragments after digestion with HincII (Figures 1Bii and 1E, arrowheads). These fragments appear transiently, likely because they undergo resection and/or strand invasion into the sister chromatid (Figure 1Biii). In contrast, no 3.6-kb and 2.0-kb incision products were detected during pICL^{Pso} repair (Figure 1E, lanes 8–14). As shown previously (Knipscheer et al., 2009), when FANCI-D2 was immunodepleted from egg extracts (Figure S1H), pICL^{Pt} accumulated as figure 8 DNA structures, and supercoiled product was less abundant, consistent with an incision defect (Figure 1F, lanes 7–12). In contrast, FANCI-D2 depletion had almost no effect on the accumulation of open circular and supercoiled pICL^{Pso} products (Figure 1F, lanes 19–24), even though the psoralen-ICL induced FANCD2 ubiquitylation (Figure S1I). In summary, the data indicate that a psoralen-ICL is unhooked by an incision-independent pathway that does not involve a DSB intermediate or require FANCI-D2.

Translesion DNA Synthesis Is Required for Gap Filling of Both Daughter Molecules

We envisioned two mechanisms of psoralen-ICL unhooking without incisions. First, in a process analogous to photoreversal (Cimino et al., 1986), the cyclobutane ring between the thymine and psoralen is broken (Figure 2A, left, blue arrowheads). This reaction would yield a psoralen mono-adduct on one strand and an undamaged thymine on the other strand (Figure 2A, middle). Alternatively, one of the two *N*-glycosyl bonds between a damaged thymine and a sugar is cleaved (Figure 2A, left, red arrowhead), generating an AP site on one parental strand and a thymine-psoralen mono-adduct on the other strand (Figure 2A, right). The first model predicts that after unhooking, gap filling on only one daughter molecule should require translesion DNA synthesis (not shown), whereas the second model predicts gap filling on both daughters requires TLS (Figure 2B). To distinguish between the models, we immunodepleted the TLS DNA polymerase REV1, which is required for ICL repair (Budzowska et al., 2015). In REV1-depleted egg extract (Figure 2C), the vast majority of pICL^{Pso} accumulated as gapped plasmids (Figure 2D), consistent with the second model. To examine where the leading strands stalled after REV1 depletion, we digested repair intermediates with AflIII and EcoRI (Figure 2E), which allowed us to monitor rightward and leftward leading strands on the same denaturing gel (Figure 2F). After REV1 depletion, rightward and leftward leading strands both stalled at or near the −1 position (Figure 2F, middle and bottom), and there was a strong reduction in extension products (Figure 2F, top), consistent with a lesion bypass defect on both strands. We conclude that gap

Please cite this article in press as: Semlow et al., Replication-Dependent Unhooking of DNA Interstrand Cross-Links by the NEIL3 Glycosylase, Cell (2016), http://dx.doi.org/10.1016/j.cell.2016.09.008

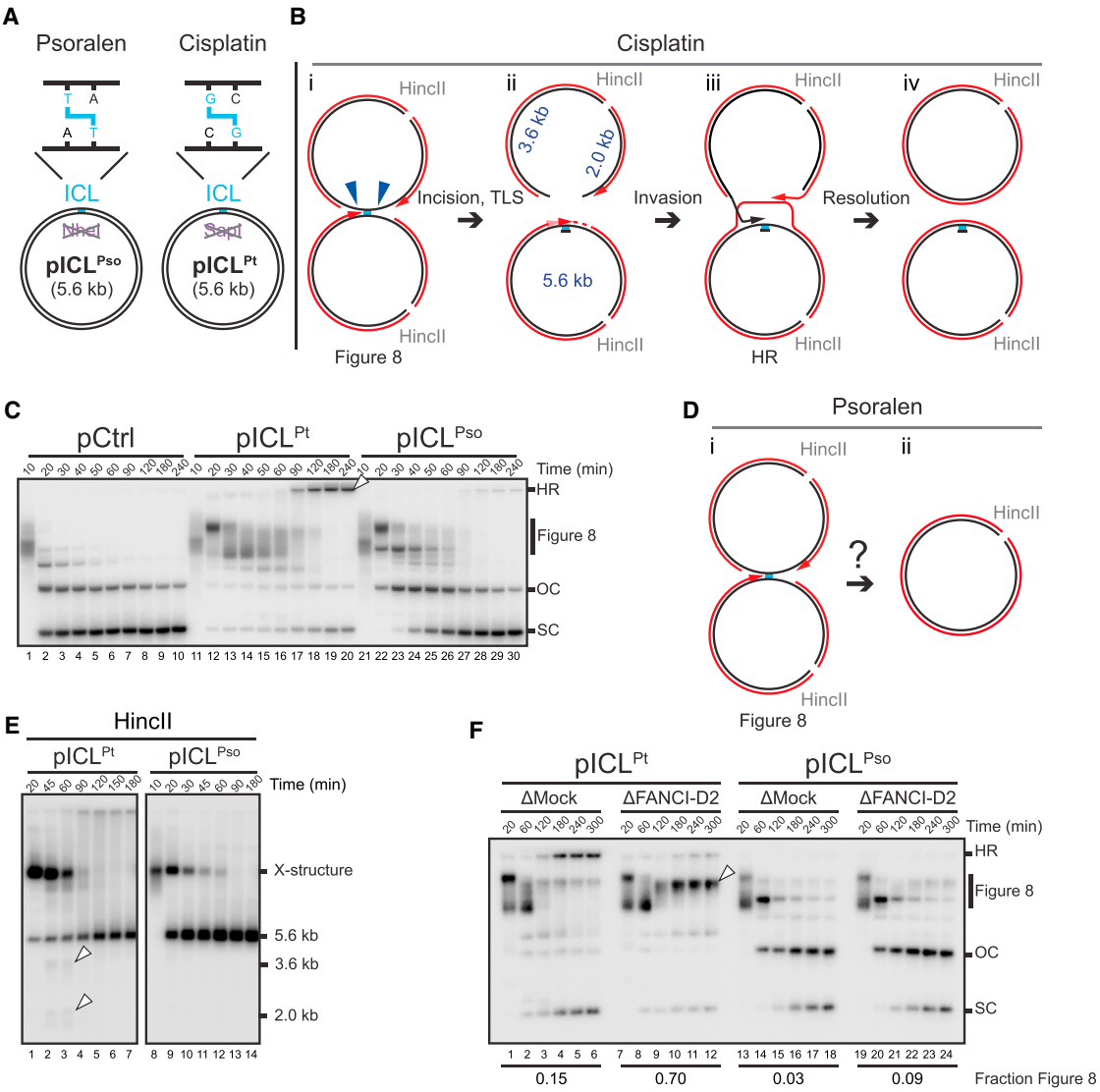

Figure 1. A Psoralen-ICL Is Unhooked by an Incision-Independent Pathway that Does Not Require FANCI-D2

(A) Cartoons of pICL^{Pso} and pICL^{Pt}. NheI and SapI restriction sites coincide with the psoralen- and cisplatin-ICLs, respectively.

(B) Cartoon of pICL^{Pt} replication intermediates digested with HincII.

(C) pCtrl, pICL^{Pt}, or pICL^{Pso} was replicated in egg extracts with [α-^{32}P]dATP. Replication intermediates were separated on a native agarose gel and visualized by autoradiography. SC, supercoiled; OC, open circular; HR, homologous recombination intermediate (also denoted by white arrowhead).

(D) Cartoon of pICL^{Pso} replication intermediates digested with HincII.

(E) pICL^{Pt} or pICL^{Pso} was replicated in egg extracts with [α-^{32}P]dATP. Replication intermediates were digested with HincII, separated on a native agarose gel, and visualized by autoradiography. White arrowheads, 3.6-kb and 2.0-kb incision products depicted in (B).

(F) pICL^{Pt} or pICL^{Pso} was replicated in mock or FANCI-D2-depleted egg extracts in the presence of [α-^{32}P]dATP, and the repair intermediates were analyzed as in (C). White arrowhead, figure 8 DNA structure. "Fraction Figure 8" indicates the proportion of figure 8 structures relative to total species at 300 min.

See also Figure S1.

filling of both daughter molecules is dependent on TLS, consistent with the *N*-glycosyl bond cleavage model (Figure 2A, right).

The Psoralen ICL Is Unhooked via *N*-Glycosyl Bond Cleavage

The *N*-glycosyl bond cleavage model predicts that an AP site is generated during psoralen-ICL unhooking (Figure 2A, right). To test this prediction, we recovered pICL^{Pso} repair intermediates and digested them with recombinant APE1, which cleaves the phosphodiester bond 5′ to an AP site. If an AP site is present near the ICL, simultaneous digestion with APE1 and HincII should yield 3.6-kb and 2.0-kb DNA fragments (Figure 2G). As shown in Figure 2H, APE1 and HincII digestion led to a substantial increase in 3.6-kb and 2.0-kb fragments relative to HincII digestion alone (lanes 15–28, quantified in Figure S1J). Disappearance of these fragments at later times (Figure 2H, lanes 27

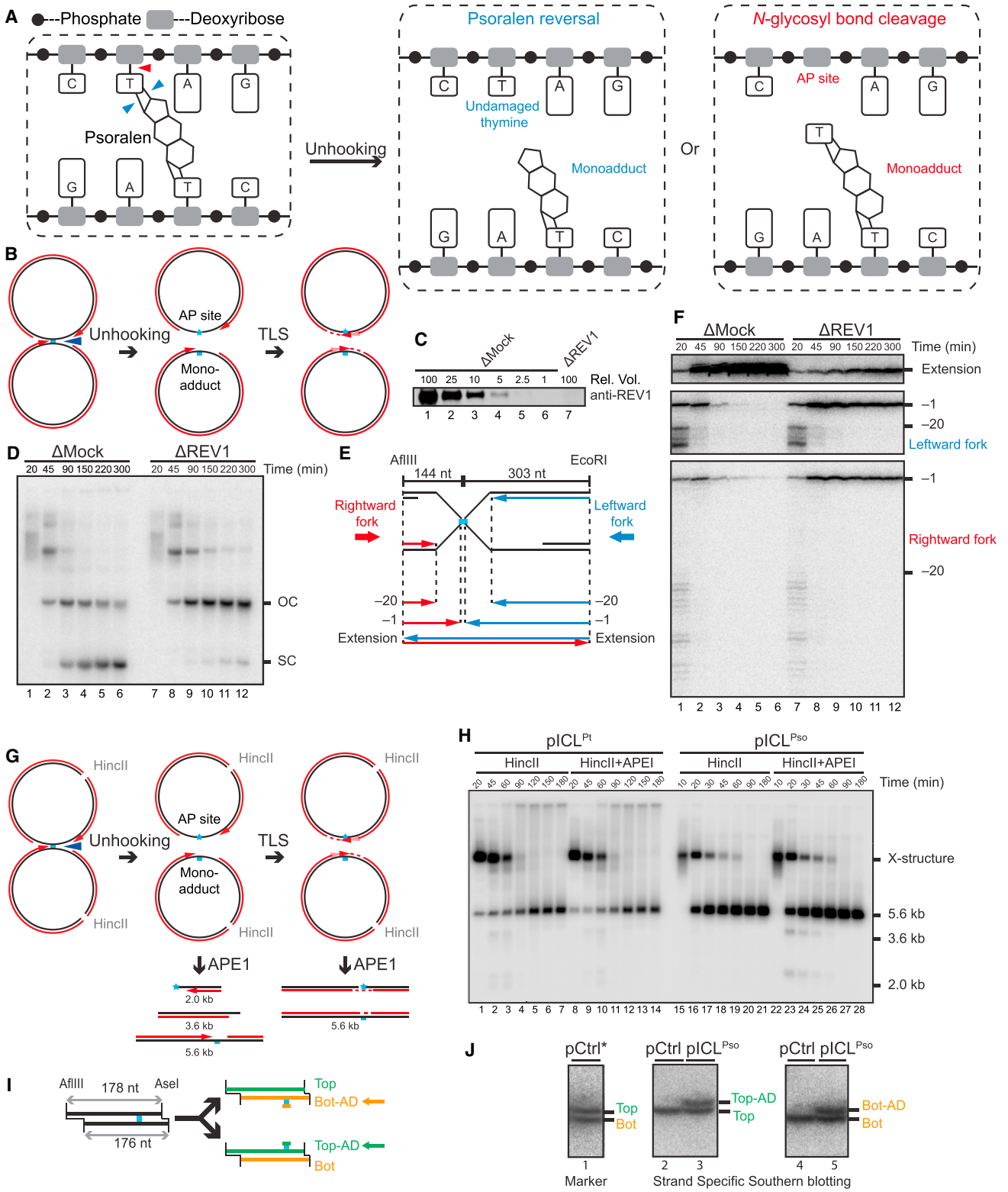

Figure 2. Psoralen ICL Is Unhooked via the Cleavage of a DNA *N*-Glycosyl Bond

(A) Two possible incision-independent unhooking pathways for a psoralen-ICL. Blue arrowheads (left) show unhooking of a psoralen-ICL via breakage of the cyclobutane ring (psoralen reversal), resulting in an undamaged thymine and a mono-adduct (middle). The red arrowhead (left) shows psoralen-ICL unhooking via cleavage of a DNA *N*-glycosyl bond, resulting in an AP site and a mono-adduct (right).

(legend continued on next page)

and 28) resulted from translesion DNA synthesis past the AP site, after which APE1 cleavage of one strand does not create a DSB (Figure 2G). In contrast, during cisplatin-ICL repair, APE1 digestion did not increase the basal level of 3.6-kb and 2.0-kb DNA fragments that arise from FANCI-D2-dependent incisions (Figures 2H, lanes 1–14, and S1J). We conclude that AP sites are specifically generated near the lesion during psoralen-ICL repair.

We also examined whether there is a mono-adduct attached to the unhooked parental strand, as predicted for *N*-glycosyl bond cleavage (Figure 2A, right). If the two *N*-glycosyl bonds are cleaved with equal probability, the mono-adduct should be detected on both parental strands. To test this idea, we digested final pICL^{Pso} repair products with AflIII and AseI so that the unmodified top and bottom strands differed by 2 nt (Figure 2I), allowing us to differentiate them on a denaturing polyacrylamide gel (Figure 2J, lane 1). After replication of pICL^{Pso} and digestion with AflIII and AseI, we detected the top and bottom parental strands, respectively, by strand-specific Southern blotting. As shown in lanes 3 and 5 of Figure 2J, both parental strands contained a mono-adduct. Collectively, our data strongly argue that the psoralen-ICL is unhooked via cleavage of one of the two *N*-glycosyl bonds forming the cross-link.

Switching between Repair Pathways

Although we detected APE1 cleavage products in every pICL^{Pso} repair reaction examined, the amount varied between experiments (data not shown). Therefore, to further examine whether the *N*-glycosyl bond is cleaved (Figure 2A), we made a new plasmid in which the psoralen cross-link is formed between two 2′-fluoroarabino-dT nucleotides (pICL$^{FdT\text{-}Pso}$; Figure 3A). The 2′ fluorine renders the thymidine *N*-glycosyl bond resistant to enzymatic cleavage (Maiti et al., 2009) and should therefore inhibit the *N*-glycosyl bond cleavage pathway. Strikingly, when pICL$^{FdT\text{-}Pso}$ was replicated in egg extracts, figure 8 structures were still resolved, but the repair intermediates included HR structures and thus much more closely resembled those of pICL^{Pt} than pICL^{Pso} (Figure 3B). Accordingly, in FANCI-D2-depleted extract (Figure S2A), pICL$^{FdT\text{-}Pso}$ accumulated as figure 8 structures (Figure 3C, arrowhead), as seen for pICL^{Pt} (Figure S2B; Knipscheer et al., 2009), and leading strands stalled at the −1 position (Figure S2C). These data confirm that the psoralen-ICL formed between normal thymidines is unhooked via cleavage of the *N*-glycosyl bond. Moreover, when the *N*-glycosyl bond cannot be cleaved, the psoralen-ICL is unhooked via FANCI-D2-dependent incisions, which appear to function as a backup repair pathway (Figure S3).

CMG Unloading Is Not Required for Psoralen-ICL Unhooking

We previously showed that during pICL^{Pt} replication, CMG unloading is required to allow a leading-strand approach to the −1 position and for ICL repair (Long et al., 2014). To address whether CMG unloading is also required for psoralen-ICL repair, we first sought a convenient and specific means to inhibit CMG unloading. Because the P97 ATPase is required for CMG unloading during DNA replication termination (Maric et al., 2014; Moreno et al., 2014), we reasoned it might also extract CMG from forks stalled at ICLs. To test this idea, we added NMS-873, an allosteric inhibitor of P97 (Magnaghi et al., 2013), to egg extracts. As shown by chromatin pull-down, NMS-873 blocked the unloading of CMG from an undamaged plasmid, as expected from a defect in termination (Figure S4A), and from pICL^{Pt} (Figure 4A, left). Under these conditions, pICL^{Pt} repair intermediates accumulated as figure 8 structures (Figure 4B, lanes 6–10), and leading strands stalled at the −20 position (Figure 4C, lanes 6–10). Strikingly, although NMS-873 also prevented CMG unloading from pICL^{Pso} (Figure 4A, right), unhooking was unaffected (Figure 4B, lanes 11–20). In the presence of NMS-873, leading strands also did not arrest at the −20 position (Figure 4C, lanes 16–20), presumably because psoralen-ICL unhooking allowed CMG to travel beyond the ICL, permitting extension of the leading strand to the ICL (Figures S3i and S3ii). On the other hand, NMS-873 efficiently blocked unhooking and leading-strand extension on pICL$^{FdT\text{-}Pso}$ (Figures S4B and S4C), demonstrating that repair of this template requires CMG unloading, as expected given its dependence on FANCI-D2-dependent incisions. Thus, CMG unloading is essential for ICL repair via the incision pathway, but not the *N*-glycosyl bond cleavage pathway.

In conclusion, a psoralen-ICL is repaired in *Xenopus* egg extract via cleavage of the *N*-glycosyl bond, CMG bypass, and TLS-dependent gap filling (Figures S3i–S3iii). The AP site is probably then removed via endogenous AP endonuclease and lyase activities (Figure S3iv), while the mono-adduct may be

(B) Model for pICL^{Pso} unhooking via cleavage of a DNA *N*-glycosyl bond, which necessitates gap filling of both daughter molecules by TLS.
(C) Mock-depleted and REV1-depleted NPE were analyzed by REV1 western blotting. A relative volume of 100 corresponds to 0.25 μL NPE.
(D) pICL^{Pso} was replicated in mock- or REV1-depleted egg extracts in the presence of [α-^{32}P]dATP. Repair intermediates were analyzed as in Figure 1C.
(E) Schematic illustration of nascent leading strands liberated after digestion of pICL^{Pso} with AflIII and EcoRI.
(F) pICL^{Pso} was replicated in mock- or REV1-depleted egg extracts in the presence of [α-^{32}P]dATP. Samples were purified and digested with AflIII and EcoRI before separation on a denaturing polyacrylamide gel. Three portions of the autoradiograph are shown with different contrasts for optimal display.
(G) Expected species after digestion of pICL^{Pso} replication intermediates with HincII and APE1, including 3.6-kb and 2.0-kb fragments.
(H) pICL^{Pt} or pICL^{Pso} was replicated in egg extracts with [α-^{32}P]dATP. Replication intermediates were digested with HincII and APE1, separated on a native agarose gel, and visualized by autoradiography. Quantification of 3.6-kb and 2.0-kb fragments is presented in Figure S1J.
(I) Depiction of final repair products after AflIII and AseI digestion. AflIII and AseI generate different-sized overhangs, allowing separation of top (178 nt) and bottom (176 nt) strands. Depending on which *N*-glycosyl bond is cleaved, the mono-adduct is present on the bottom (Bot-AD) or top (Top-AD) strands.
(J) Detection of pICL^{Pso} mono-adducts. pCtrl or pICL^{Pso} was replicated for 3 hr in egg extract. DNA was isolated, digested with AflIII and AseI, separated on a denaturing sequencing gel, and analyzed by strand-specific Southern blotting to visualize the top strand (middle) or bottom strand (right). The absence of bottom (lane 2) or top strands (lane 4) in the Southern blot of pCtrl indicates the strand specificity of the blotting protocol. To generate size markers for the top (178 nt) and bottom (176 nt) strands (left panel, lane 1), pCtrl was replicated in the presence of [α-^{32}P]dATP (pCtrl*) and analyzed on the same sequencing gel after AflIII and AseI digestion.

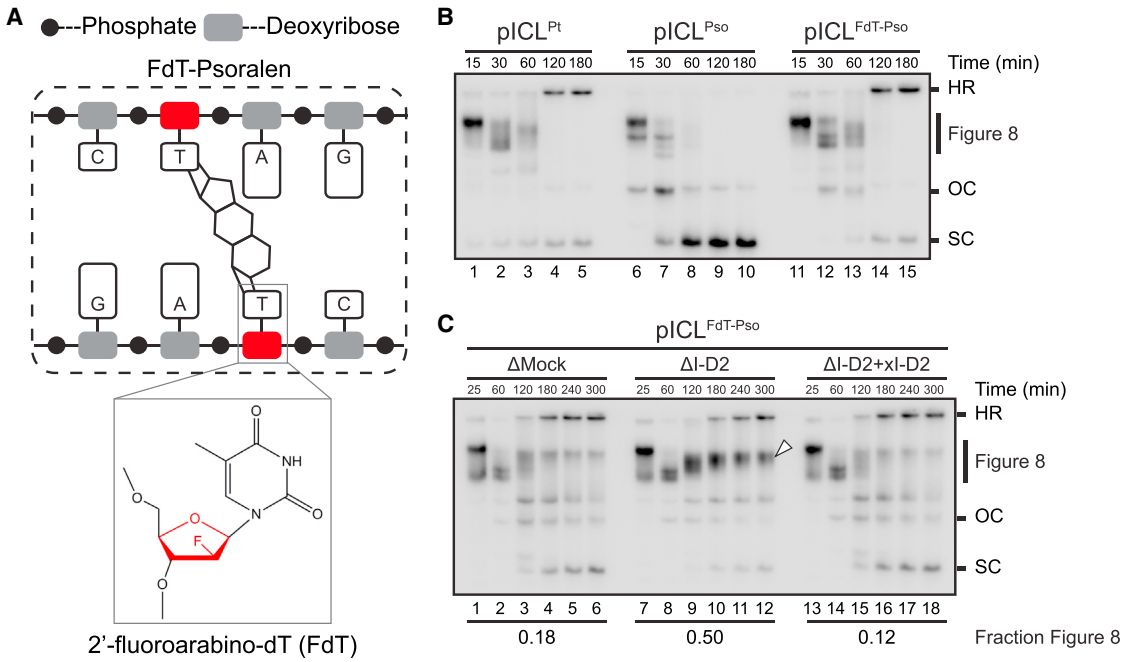

Figure 3. Psoralen-ICL Undergoes FANCI-D2-Dependent Processing When the *N*-glycosyl Bond Cannot Be Cleaved

(A) Schematic of a psoralen-ICL formed between two 2′-fluoroarabino-dT (FdT) nucleosides (inset).

(B) pICL^{Pt}, pICL^{Pso}, or pICL$^{FdT\text{-}Pso}$ was replicated in egg extracts in the presence of [α-^{32}P]dATP. Repair intermediates were analyzed as in Figure 1C.

(C) pICL$^{FdT\text{-}Pso}$ was replicated in mock-depleted egg extract, FANCI-D2-depleted extract (ΔI-D2), or ΔI-D2 extract supplemented with xFANCI-D2 (ΔI-D2 + xI-D2) in the presence of [α-^{32}P]dATP, and the repair intermediates were analyzed as in Figure 1C. White arrowhead, figure 8 DNA structure that persists in the absence of FANCI-D2. "Fraction Figure 8" indicates the proportion of figure 8 structures relative to total species at 300 min.

See also Figures S2 and S3.

removed via base excision repair (Couvé et al., 2009). When the *N*-glycosyl bond cannot be cleaved, psoralen-ICL repair proceeds via the classic, FANCI-D2-dependent incision pathway that requires CMG unloading (Figures S3v–S3ix).

Repair of an AP-ICL by Incision-Dependent and Incision-Independent Pathways

We next wished to examine an ICL that might form in cells. AP sites in DNA comprise an equilibrating mixture of structures, including a ring-open aldehyde that can react with the exocyclic amine of a nucleobase on the opposite strand, generating an AP-ICL through a non-native *N*-glycosyl bond (Figure 5A; Price et al., 2015). AP sites react most efficiently with adenines on the other strand that are displaced by one residue to the 3′ side (Figure 5B). Given the high abundance of AP sites in cells and considerable stability of AP-ICLs ($t_{1/2}$, ~3 days at 37°C; Price et al., 2015), AP-ICLs may represent physiologically relevant impediments to DNA replication.

We generated a plasmid containing a site-specific AP-ICL (pICL^{AP}; Figures 5B and S1B) and incubated it in egg extract. Both unhooking and error-free repair of the AP-ICL was replication dependent (Figures S1C, S1D, S5A, and S5B). The amount of pICL^{AP} repair products (43%) was much greater than the amount (5%) observed for pICL^{Pso} (compare Figures S5B and S1G; see Discussion). As seen for pICL^{Pso}, the majority of pICL^{AP} figure 8 molecules were converted directly to gapped and supercoiled species (Figure 5C). However, a minor fraction accumulated in the well as HR products (arrowhead). These data suggest that a minority of pICL^{AP} molecules were unhooked via incisions (as for pICL^{Pt}), and a majority might be unhooked via the *N*-glycosyl bond cleavage pathway (as for pICL^{Pso}). Consistent with this interpretation, we detected a modest accumulation of figure 8 molecules in FANCI-D2-depleted egg extract (Figures 5D, arrowhead, and S5C). However, FANCI-D2 depletion had almost no effect on the formation of nicked and supercoiled molecules (Figure 5D), indicating that the bulk of pICL^{AP} unhooking is FANCI-D2- and incision-independent. We conclude that a small fraction of pICL^{AP} is unhooked via FANCI-D2-dependent incisions, whereas the majority is unhooked by an alternative mechanism.

To gain additional insight into pICL^{AP} repair, we examined nascent-strand products (Figure 5E). As shown in Figure 5F, both the leftward and rightward leading strands stalled transiently near the −20 position before being converted to longer products (lanes 13–18). For the leftward leading strand, which encounters the AP side of the ICL (Figure 5E), stalling near −20 was followed by a strong but transient arrest at the −1 position (Figure 5F, white arrowhead), suggesting that unhooking of pICL^{AP} generates a lesion whose bypass requires TLS. For the rightward leading strand, which encounters the adenosine side of the ICL (Figure 5E), stalling near −20 was also followed by a −1 arrest (black arrowhead). However, these −1 products

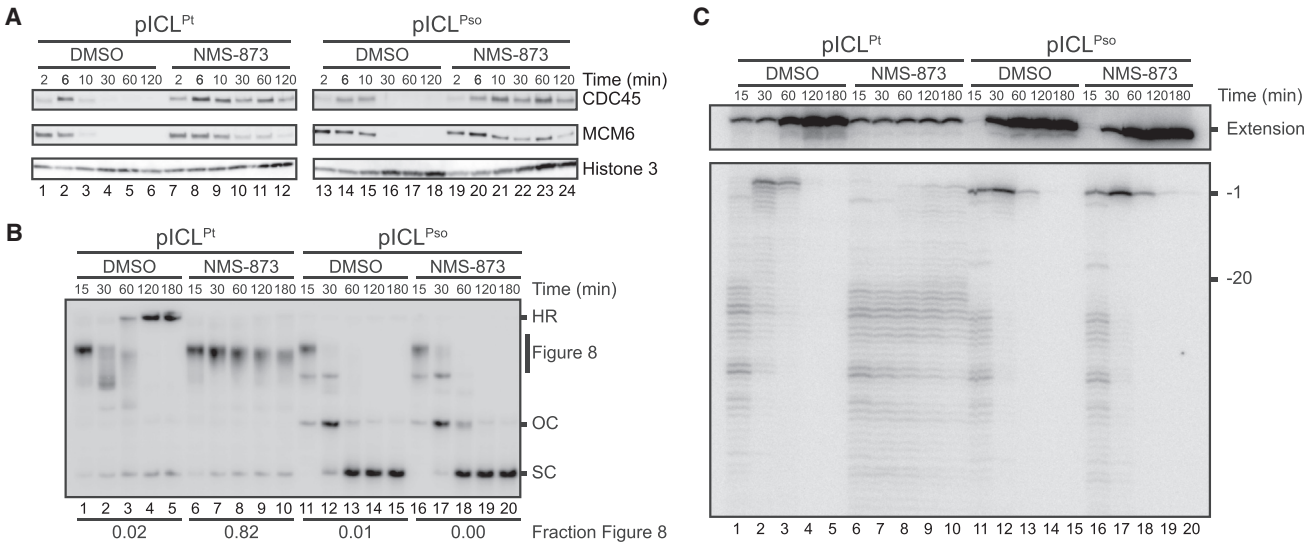

Figure 4. CMG Unloading Is Not Required for Psoralen-ICL Unhooking

(A) pICL^{Pt} or pICL^{Pso} (containing 48 *lacO* repeats) was replicated in the presence or absence of NMS-873 and, at the indicated times, pulled down using LacI-coated beads. Western blotting was performed on chromatin samples with the indicated antibodies.

(B) pICL^{Pt} and pICL^{Pso} were replicated in the presence or absence of NMS-873 with [α-^{32}P]dATP, and repair intermediates were analyzed as in Figure 1C. "Fraction Figure 8" indicates the proportion of figure 8 structures relative to total species at 180 min.

(C) DNA samples from (B) were digested with AflIII and EcoRI before separation on a denaturing polyacrylamide gel. Extension products and rightward fork products (see Figure 2E) are shown with different contrast for optimal display.

See also Figure S4.

accumulated more slowly than those of the leftward fork and to a lesser extent. This suggests that the rightward −1 products might derive from the small fraction of pICL^{AP} molecules that undergo CMG unloading, incisions, and TLS bypass of the resulting mono-adduct (compare accumulation of rightward −1 products for pICL^{Pt} [Figure 5F, lanes 1 to 4] and pICL^{AP} [Figure 5F, lanes 13–16]). To test this idea, we added the P97 inhibitor NMS-873 to suppress the incision pathway. As seen for pICL^{Pso} (Figure 4B), NMS-873 strongly inhibited CMG unloading from pICL^{AP} (Figure S5D) but had no effect on unhooking (Figure S5E, lanes 19–24). Importantly, while NMS-873 had no significant effect on the leftward leading strand, it completely abolished −1 arrest of the rightward leading strand (Figure 5F, lanes 19–24), consistent with formation of this product requiring CMG unloading. In support of the −1 product entering the incision pathway, FANCI-D2 depletion led to its persistence (Figure S5F). Our results show that a small fraction of pICL^{AP} unhooking involves CMG unloading, leading strand advance to −1, and FANCI-D2-dependent incisions, as seen for pICL^{Pt} and pICL$^{Pso\text{-}FdT}$. However, pICL^{AP} is unhooked predominantly by an incision-independent pathway that does not require CMG unloading.

We next addressed whether incision-independent AP-ICL unhooking involves enzymatic cleavage of an *N*-glycosyl bond. Consistent with this idea, pICL^{AP} repair intermediates were sensitive to APE1 digestion (Figures 6A–6C), indicating that unhooking of pICL^{AP} generates an AP site. The AP-ICL contains two distinct *N*-glycosyl bonds, either of which could be cleaved (Figures 5A and 6D). To distinguish which *N*-glycosyl bond is cleaved, we depleted REV1 from egg extract (Figure 6E) and examined pICL^{AP} replication in the presence of NMS-873 to suppress the incision pathway. As shown in Figure 6F, in the absence of REV1, roughly half of the unhooked plasmids accumulated as open circular molecules, indicating that synthesis of only one nascent strand requires TLS, as predicted for cleavage of the non-native *N*-glycosyl bond (Figure 6D, red pathway). Strikingly, in the absence of REV1, the leftward leading strand, which encounters the AP side of the ICL, stalled at the −1 position (Figure 6G, top), whereas the rightward leading stand, which encounters the adenine side of the ICL, exhibited no −1 arrest (Figure 6G, bottom). These data further argue that the AP-ICL is unhooked via enzymatic cleavage of the non-native *N*-glycosyl bond to regenerate an AP site and an undamaged adenosine (Figure 6D, red pathway). As seen for cisplatin- and psoralen-ICLs (Zhang et al., 2015), AP-ICL unhooking requires replication fork convergence (Figure S6).

NEIL3 Unhooks Psoralen and AP ICLs

We next sought to identify the DNA glycosylase that unhooks psoralen- and AP-ICLs. In an unrelated mass spectrometry analysis of undamaged plasmid replicating in egg extracts, we identified NEIL3 as a possible replisome component (unpublished data). NEIL3 is one of eleven annotated glycosylases in the *Xenopus* genome and a member of the Fpg/Nei glycosylase family that has been implicated in the removal of oxidized bases from single-stranded DNA (ssDNA; Liu et al., 2013a). We raised an antibody to *Xenopus* NEIL3 and depleted it from egg extracts (Figure S7A). Replication of undamaged or cisplatin-ICL-containing plasmids was unaffected by NEIL3 depletion (Figure S7C). In contrast, depletion of NEIL3 led to a reduction

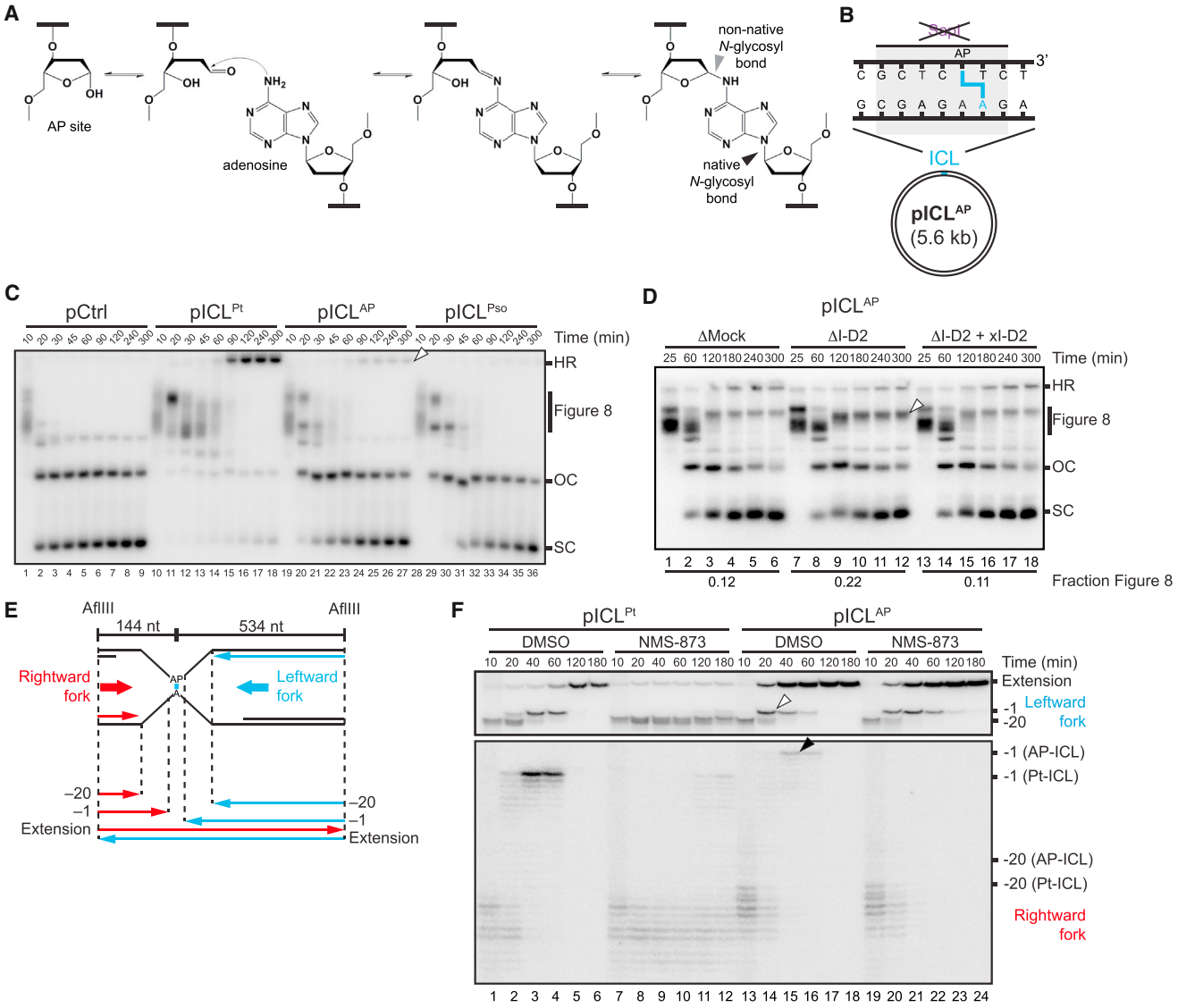

Figure 5. An AP-ICL Is Repaired by an Incision-Independent Pathway that Does Not Require FANCI-D2 or CMG Unloading

(A) Mechanism of AP-ICL formation.

(B) Cartoon of an AP-ICL containing plasmid (pICL^{AP}), in which the SapI restriction site coincides with the ICL.

(C) pCtrl, pICL^{Pt}, pICL^{AP}, or pICL^{Pso} was replicated in egg extracts and analyzed as in Figure 1C. White arrowhead, homologous recombination intermediate that accumulates for pICL^{AP}.

(D) pICL^{AP} was replicated in mock-depleted egg extract, FANCI-D2-depleted extract (ΔI-D2), or ΔI-D2 extract supplemented with xFANCI-D2 (ΔI-D2+xI-D2), and analyzed as in Figure 1C. White arrowhead, figure 8 structures that persist in the absence of FANCI-D2. "Fraction Figure 8" indicates the proportion of figure 8 structures relative to total species at 300 min.

(E) Schematic illustration of nascent leading strands liberated by digestion of pICL^{AP} with AflIII.

(F) pICL^{Pt} and pICL^{AP} were replicated with [α-^{32}P]dATP in the presence or absence of NMS-873. The nascent strands were purified and digested with AflIII before separation on a denaturing polyacrylamide gel. Two portions of the autoradiograph are shown with different contrasts for optimal display. White arrowhead, leftward −1 products. Black arrowhead, rightward −1 products.

See also Figure S5.

in pICL^{Pso} and pICL^{AP} open circular and supercoiled DNA products and caused accumulation of these plasmids as figure 8 structures and slowly migrating species resembling the HR reaction intermediates of pICL^{Pt} (Figure 7A, lanes 7–12 and 31–36). The effect of NEIL3 depletion was reversed by recombinant wild-type NEIL3, but not catalytically deficient NEIL3-K60A (Figure 7A, lanes 13–24 and 37–48, and Figure S7B; Krokeide et al., 2013). Thus, despite being structurally distinct, both psoralen- and AP-ICLs are unhooked by NEIL3. When NEIL3-depleted extracts were supplemented with NMS-873 to inhibit

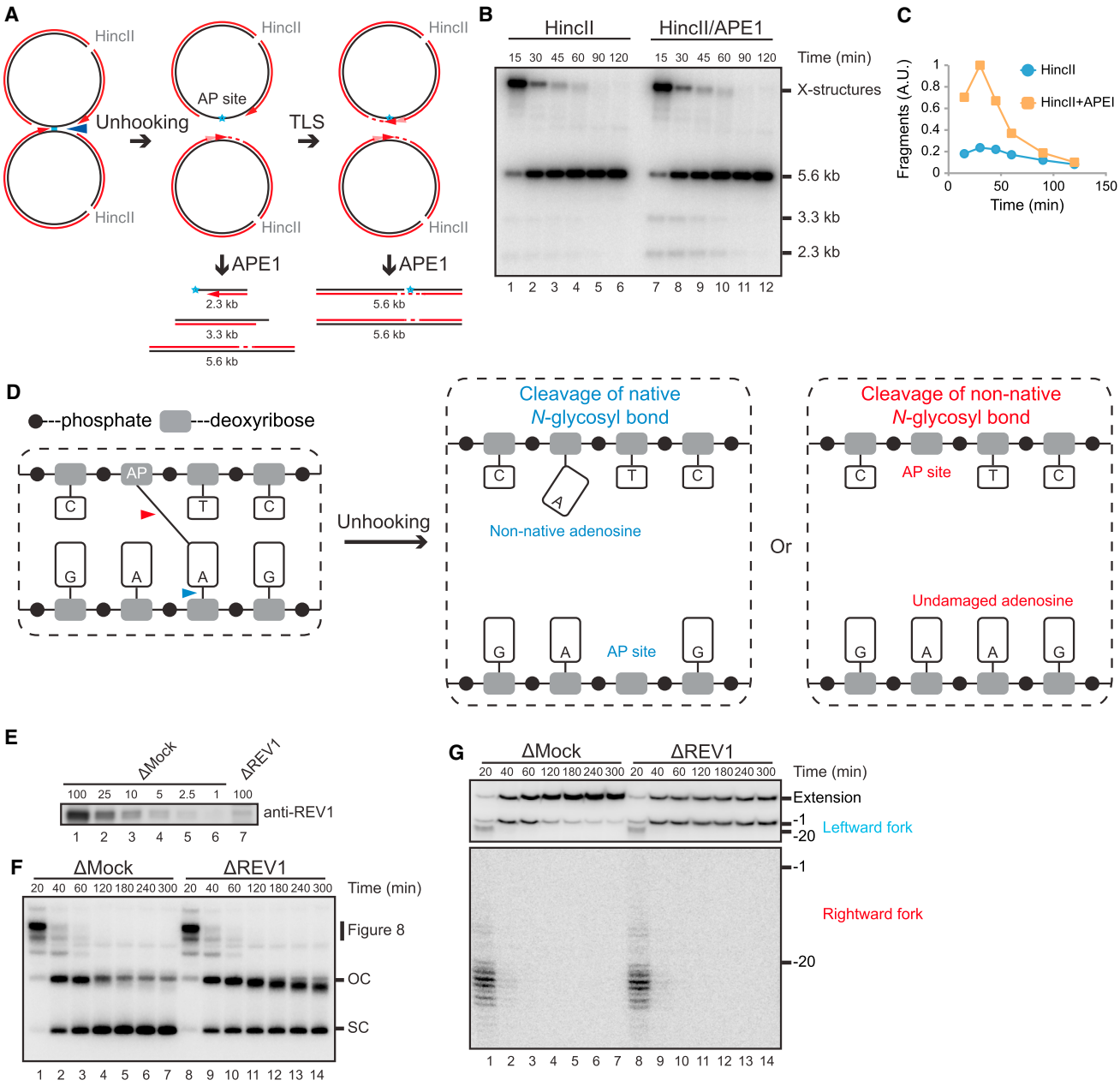

Figure 6. An AP-ICL Is Unhooked via Cleavage of the Non-native *N*-Glycosyl Bond

(A) Expected species after digestion of pICL^{AP} with HincII and APE1, including 3.3-kb and 2.3-kb fragments.

(B) pICL^{AP} was replicated in egg extracts and then digested with HincII and APE1 as in Figure 2H.

(C) The 3.3-kb and 2.3-kb fragments in (B) were quantified and plotted.

(D) Two possible incision-independent unhooking pathways for an AP-ICL. Cleavage of the native *N*-glycosyl bond (blue arrowhead) yields a non-native adenosine and an AP site (middle), whereas cleavage of the non-native *N*-glycosyl bond (red arrowhead) yields an AP site and a normal adenosine (right).

(E) Mock-depleted and REV1-depleted NPE were analyzed by REV1 western blotting. A relative volume of 100 corresponds to 0.66 μL NPE.

(F) pICL^{AP} was replicated in mock- or REV1-depleted egg extract in the presence of [α-^{32}P]dATP and NMS-873 and analyzed as in Figure 1C.

(G) pICL^{AP} was replicated in mock- or REV1-depleted egg extract in the presence of [α-^{32}P]dATP and NMS-873. Samples were purified and digested with AflIII before separation on a denaturing polyacrylamide gel. Two portions of the autoradiograph are displayed with different contrast for optimal display.

See also Figure S6.

CMG unloading and the incision pathway, the low-mobility intermediates were abolished and figure 8 structures persisted for an extended period (Figure S7D, arrowheads). This result indicates that incisions and *N*-glycosyl bond cleavage represent the two major pICL^{Pso} and pICL^{AP} unhooking pathways in egg extracts.

Please cite this article in press as: Semlow et al., Replication-Dependent Unhooking of DNA Interstrand Cross-Links by the NEIL3 Glycosylase, Cell (2016), http://dx.doi.org/10.1016/j.cell.2016.09.008

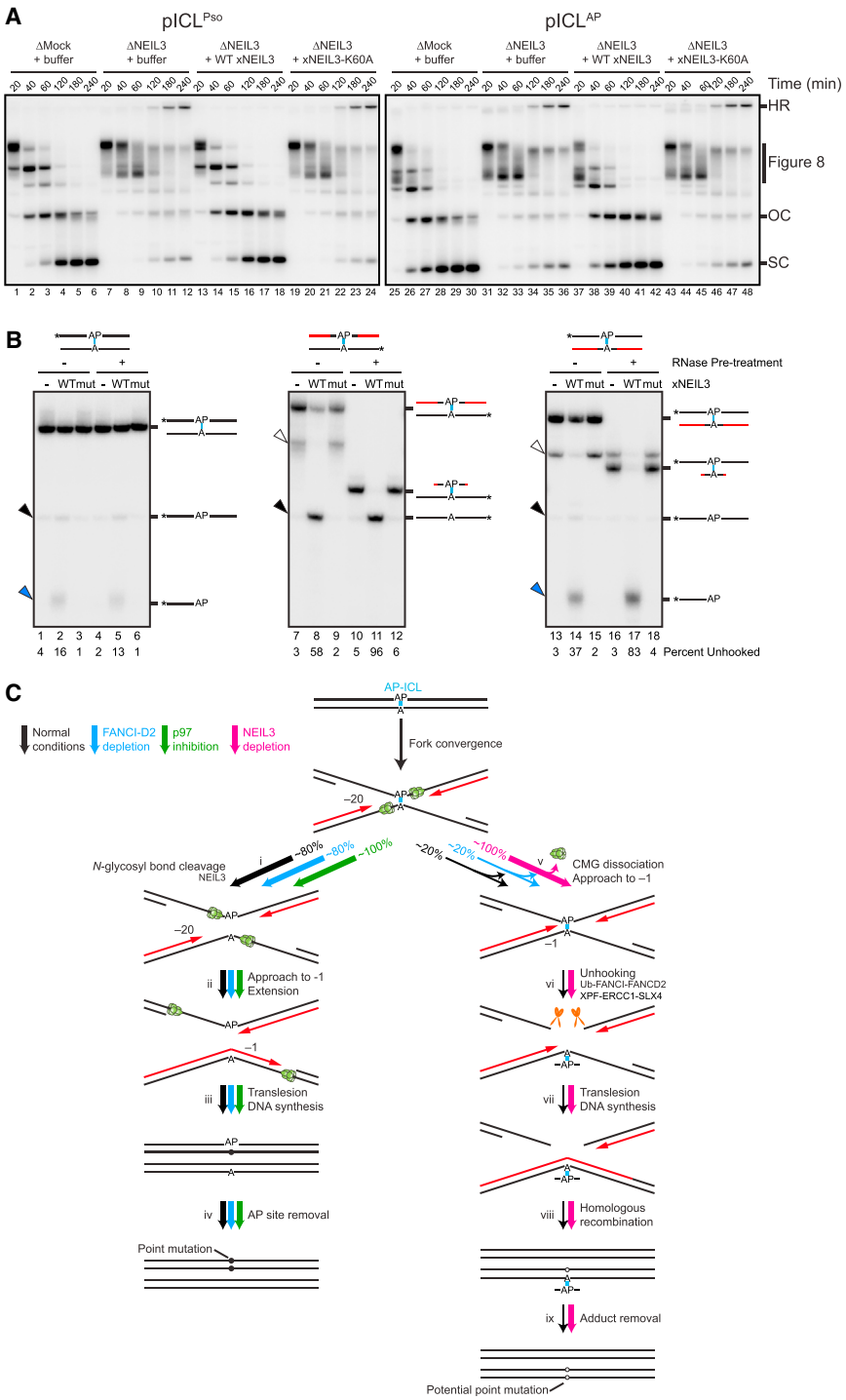

Figure 7. NEIL3 Unhooks Psoralen and AP-ICLs

(A) pICL^{Pso} or pICL^{AP} was replicated in mock-depleted, NEIL3-depleted, or NEIL3-depleted egg extract supplemented with 300 nM recombinant NEIL3 in the presence of [α-^{32}P]dATP. Repair intermediates were analyzed as in Figure 1C. As shown in Figure S7E, 15 nM recombinant NEIL3 also rescued pICL^{Pso} unhooking in NEIL3-depleted egg extract.

(B) Oligonucleotide substrates containing an AP-ICL were incubated with recombinant wild-type (WT) or K60A mutated (mut) NEIL3, separated on a denaturing polyacrylamide gel, and visualized by autoradiography. Black lines, DNA. Red lines, RNA. Cyan, AP-ICL. Asterisks indicate the ^{32}P radiolabel. Black arrowheads, unhooked ssDNA. Blue arrowheads, β-elimination cleavage product. Bands marked by white arrowheads likely represent substrate that was not denatured during electrophoresis.

(C) Model for AP-ICL repair by incision-independent (left branch) or incision-dependent (right branch) pathways. Black lines, parental DNA. Red lines, nascent leading strands. Cyan, AP-ICL. Green ovals, CMG helicase. Pathway utilization is illustrated for unmodified extract (black arrows), FANCI-D2-depleted extract (blue arrows), extract supplemented with NMS-873 (green arrows), and NEIL3-depleted extract (pink arrows). Closed circles indicate point mutations that arise due to bypass of an AP site. Open circles indicate potential point mutations that may be introduced due to bypass of an AP-ICL-derived adenine mono-adduct.

See also Figure S7.

To determine whether NEIL3 is sufficient to unhook an ICL, we incubated recombinant NEIL3 with different AP-ICL-containing oligonucleotide substrates and looked for the appearance of ssDNA (Figure 7B, black arrowheads). When the AP-ICL was located in duplex DNA, NEIL3-dependent unhooking was inefficient (Figure 7B, lane 2). To address whether the presence of ssDNA might enhance NEIL3 activity, we engineered ribonucleotides on one strand surrounding the ICL (Figure 7B, red lines) and optionally digested the substrates with RNase before addition of NEIL3. As shown in Figure 7B, the presence of RNA increased NEIL3-dependent unhooking (lane 8), and RNase digestion stimulated this activity further (lane 11). Catalytically inactive NEIL3-K60A had no activity on these substrates (Figure 7B, mut). Therefore, NEIL3 possesses intrinsic ICL unhooking activity that is stimulated by unusual double helical structure and/or ssDNA character. Notably, when the strand containing the AP site was labeled, a rapidly migrating species was detected (Figure 7B, blue arrowheads). This species arises from the AP lyase activity of NEIL3 (Liu et al., 2010), which cleaves the phosphodiester backbone, yielding a shortened ssDNA product. However, NEIL3's AP lyase activity appears to be largely irrelevant for ICL repair, because we find no evidence of DSB formation during AP-ICL unhooking in egg extract (see Discussion). Importantly, no shortened ssDNA product was detected when the bottom strand was labeled (Figure 7B, lanes 8

and 11), indicating that AP lyase activity is targeted exclusively to the top strand. Therefore, recombinant NEIL3 cleaves the non-native *N*-glycosyl bond (Figure 6D, red arrowhead), as observed in egg extracts.

Our results show that AP-ICLs are unhooked via two pathways. The minor pathway involves CMG unloading and FANCI-D2-dependent incisions (Figure 7C, thin black arrows). The major pathway, which is analogous to psoralen-ICL unhooking (Figure S3), involves cleavage of the non-native *N*-glycosyl bond by NEIL3 (Figure 7C, thick black arrows). Unhooking likely allows converging CMGs to pass over the lesion, after which the remaining gaps are filled (Figures 7Cii and 7Ciii). For the strand containing the AP site, gap filling requires REV1-dependent TLS (Figure 7Ciii). Finally, the AP site is probably removed by an AP endonuclease (Figure 7Civ).

DISCUSSION

We previously showed that *Xenopus* egg extracts repair cisplatin-ICLs via FANCI-D2-dependent incisions at stalled replication forks. Using the same cell-free system, we now report a mechanism of S phase ICL repair that operates on AP-ICLs (Figures 7Ci–7Civ), which may form in vivo, as well as psoralen-ICLs (Figures S3i–S3iv). In this pathway, after forks converge on the ICL, the lesion is unhooked via *N*-glycosyl bond cleavage by NEIL3. *N*-glycosyl cleavage is faster than incision and avoids DSB formation. When *N*-glycosyl cleavage is prevented, unhooking occurs via incisions, establishing highly flexible pathway choice. Our results identify a new mechanism of S phase ICL repair that avoids the risk of gross chromosomal rearrangements.

NEIL3 as an ICL Glycosylase

NEIL3 is a vertebrate-specific Fpg/Nei family DNA glycosylase. Although NEIL3 acts preferentially on further oxidation products of 8-oxo-dG in vitro, its biological function has remained elusive (Liu et al., 2013a). Our work now identifies a role for NEIL3 in replisome bypass of ICLs in S phase. Consistent with this idea, NEIL3 is specifically expressed in the S and G2 phases of proliferating tissues, including bone marrow, spleen, neuronal progenitor cells, and tumors (Hildrestrand et al., 2009; Neurauter et al., 2012; Torisu et al., 2005).

Most DNA glycosylases cleave the *N*-glycosyl bond only after the damaged base is rotated by ~180° into the enzyme's catalytic pocket ("eversion"; Brooks et al., 2013). The question arises how NEIL3 unhooks an ICL, given that the bases of an ICL cannot be readily everted. Notably, the structure of NEIL3's glycosylase domain is virtually superimposable on that of NEIL1 (Liu et al., 2013a), a related glycosylase that removes oxidized bases via classic base eversion. However, NEIL3 contains two features that suggest a unique mode of action. First, NEIL3 lacks two of the three NEIL1 residues that stabilize the nucleobase opposite the everted base, and it lacks the loop that stabilizes the everted base (Liu et al., 2013b). Second, the DNA binding cleft of NEIL3 contains two negatively charged patches that disfavor interactions with the DNA strand opposite the damaged base (Liu et al., 2013b), which explains NEIL3's strong preference for ssDNA damage (Liu et al., 2010). Based on these considerations, we speculate that replication fork convergence places ICLs in a ssDNA context, allowing partial eversion of the cross-linked base into the active site of NEIL3, which is unusually open. As such, NEIL3's mechanism is probably distinct from that of AlkD, a DNA glycosylase recently shown to cleave bulky base lesions in the complete absence of base eversion (Mullins et al., 2015). A recent report that *Streptomyces* orf1 DNA glycosylase can act on azinomycin-B-ICLs (Wang et al., 2016) suggests that ICL unhooking by DNA glycosylases is widely conserved in evolution.

NEIL3 is bifunctional, possessing both DNA glycosylase and AP lyase activities (Figure 7B; Krokeide et al., 2013; Liu et al., 2010). However, in the context of replication-coupled ICL repair, AP lyase activity after unhooking would create a DSB. We observed little or no evidence of DSB formation during psoralen- or AP-ICL repair, especially when NEIL3 was the sole unhooking activity (Figures 4B and S5E), implying that NEIL3's AP lyase activity is suppressed during ICL repair. We speculate that once NEIL3 has unhooked the ICL, CMG or some other factor displaces NEIL3 from DNA, preventing the lyase reaction.

Pathway Choice during ICL Repair

We showed that upon chemical stabilization of *N*-glycosyl bonds or depletion of NEIL3, psoralen- and AP-ICLs switched pathways and were now processed via FANCI-D2-dependent incisions (Figures S3 and 7C, pink arrows). Conversely, when incisions were blocked during AP-ICL repair (with NMS-873), all repair occurred via *N*-glycosyl cleavage (Figure 7C, green arrows). Therefore, for these two lesions, there is considerable flexibility in which pathway is utilized for repair. NEIL3-mediated *N*-glycosyl cleavage is the primary mechanism, probably because it does not require CMG unloading or FANCI-D2 activation, and therefore occurs more rapidly than incisions. We previously reported that, like a cisplatin-ICL, a nitrogen-mustard-like-ICL is unhooked via incisions (Räschle et al., 2008). However, this ICL was generated between 7-deaza-2′-deoxyguanosines to counteract the inherent instability of the *N*-glycosyl bond in N7-alkylated guanines (Guainazzi et al., 2010). This stabilized nitrogen-mustard-ICL might resist the action of an ICL glycosylase, channeling the lesion into the incision-dependent pathway. Therefore, of the four ICLs we have examined so far, cisplatin-ICLs are the only ones that are clearly refractory to *N*-glycosyl bond cleavage. This feature of cisplatin-ICLs might result from the massive distortion of the DNA induced by the lesion. It should be noted that *Neil3* nullizygous murine embryonic fibroblasts (MEFs) exhibit modest sensitivity to cisplatin (Rolseth et al., 2013), suggesting that a portion of cisplatin-ICLs may be processed by NEIL3 in cells. More ICLs will have to be examined to determine whether the degree of distortion is a primary factor in determining pathway choice.

Given our observation that *N*-glycosyl bond cleavage is an efficient means of repairing psoralen-ICLs, why does FANCD2 deficiency cause hypersensitivity to psoralen in *Caenorhabditis elegans*, mouse, and human cells (Houghtaling et al., 2005; Lee et al., 2007; Rothfuss and Grompe, 2004)? There are several possibilities. First, the number of ICLs generated in clonogenic survival experiments may overwhelm NEIL3, leading to a requirement for FANCI-D2-dependent unhooking. Second, psoralen-ICLs may usually be processed via *N*-glycosyl

unhooking, but a fraction may not be compatible with this pathway due to local DNA or chromatin structure, requiring incisions. This concept is illustrated by AP-ICL processing in egg extracts, which occurs by both pathways (Figure 7C). Even in the case of pICL^{Pso}, FANCI-D2 depletion stabilized a small population of figure 8 molecules (Figure 1F, lanes 19–24), indicating the incision pathway also operates on a minor fraction of these lesions. This observation is consistent with the recruitment of FANC proteins to chromatin in a recent proteomic analysis of psoralen-ICL repair (Räschle et al., 2015). Finally, FANCD2 may play at least one other role in ICL repair that is independent of unhooking. Importantly, the severe phenotype observed in humans lacking *FANC* genes (Joenje and Patel, 2001) shows that glycosylase-mediated unhooking does not fully substitute for incisions in the processing of endogenous lesions. It is important to note that like FANC-deficient mice, *Neil3* nullizygous mice exhibit no severe phenotypes (Sejersted et al., 2011; Torisu et al., 2005), raising the possibility that these two repair systems have overlapping functions. Future experiments will address the relative roles of incision versus *N*-glycosyl bond cleavage in the response to exogenous and endogenous ICLs.

Mutagenic Potential of Different ICL Repair Strategies

We showed previously that cisplatin-ICL repair is ~98% error-free, because after incisions, bypass of the liberated mono-adduct is quite accurate (Budzowska et al., 2015). This can be explained if bypass utilizes DNA pol eta, which prefers to insert cytidines across from guanosine-cisplatin adducts (Alt et al., 2007). Although cisplatin-ICL repair appears to generate relatively little point mutagenesis, it involves a DSB intermediate, which can lead to gross chromosomal rearrangements, a hallmark of cancer. The mutagenic potential of the NEIL3 pathway is very different. After *N*-glycosyl bond cleavage of a psoralen-ICL, one parental strand retains an AP site, whereas the other contains a thymidine-psoralen mono-adduct (Figure S3, black arrows). Although we have not determined the fidelity of psoralen-ICL repair, it is likely to be low, since the AP site is non-instructive (Liao et al., 2007). Consistent with this prediction, the efficiency of error-free repair, as measured by restriction-site regeneration, is only ~5%: the mono-adduct (which is not removed in egg extracts) blocks the restriction site in half the unhooked plasmids, and random nucleotides are inserted across from the AP site in the other half (Figure S3iii). Repair should be further reduced by the fact that not all AP sites are removed after lesion bypass (Figure S3iv). In contrast, after *N*-glycosyl unhooking of the AP-ICL, one sister carries an AP site and the other a normal adenosine (Figure 7Ci). Bypass of the AP site should be highly mutagenic, as for the psoralen-ICL, but the adenosine will be copied accurately without TLS (Figure 7Cii). Accordingly, error-free AP-ICL repair is much more efficient than error-free psoralen-ICL repair (approaching 50%). In summary, cisplatin-ICL repair involves low point mutagenesis but a high potential for gross chromosomal rearrangements, whereas *N*-glycosyl bond unhooking likely involves high point mutagenesis while avoiding translocations.

N-glycosyl Bond Cleavage and CMG Dynamics

Cisplatin-ICL unhooking requires replication fork convergence to allow CMG unloading and FANCI-D2-dependent incision by XPF-ERCC1 (Klein Douwel et al., 2014; Knipscheer et al., 2009; Zhang et al., 2015). NEIL3-dependent unhooking of psoralen- (Zhang et al., 2015) and AP-ICLs (Figure S6) also requires fork convergence. However, in this case, CMG unloading is not essential for repair. Instead, CMG may actually be required for *N*-glycosyl bond cleavage. When CMG unloading was blocked during AP-ICL repair with P97 inhibitor, the incision pathway was abolished, and all the ICLs were processed via *N*-glycosyl bond cleavage (Figure 7C, green arrows). In contrast, in FANCI-D2-depleted extract (where CMG unloading is unaffected; Figure S5F), unincised AP-ICLs remained trapped as figure 8 structures and were not processed by NEIL3 (Figure 7C, thin blue arrow). We speculate that once CMG dissociation commits a lesion to the incision pathway, NEIL3 cannot cleave the *N*-glycosyl bond. In this scenario, CMG might recruit NEIL3 to the ICL and/or maintain an appropriate DNA structure for NEIL3 action. The dependence of unhooking on converged CMGs would insure that NEIL3 does not accidentally attack bases at single, active replication forks. After *N*-glycosyl bond cleavage, CMGs probably translocate past the unhooked ICL until they reach the downstream Okazaki fragment of the converged fork, whereupon they dissociate via the mechanism that operates during termination (Figures S3i–S3iii and 7Ci–7Ciii; Dewar et al., 2015).

CONCLUSIONS

In contrast to the current view that eukaryotic ICL unhooking necessarily involves endonucleolytic incisions, we show that ICLs can also be unhooked via *N*-glycosyl cleavage by the NEIL3 glycosylase. This reaction does not require CMG unloading, mobilization of the Fanconi pathway, or a DSB break intermediate and is therefore fast while also avoiding the risk of gross chromosomal rearrangements. Therapeutically, inactivation of NEIL3 in cancer patients might enhance the efficacy of chemotherapy, whereas upregulation of NEIL3 may ameliorate the symptoms of Fanconi anemia.

STAR★METHODS

Detailed methods are provided in the online version of this paper and include the following:

- KEY RESOURCES TABLE
- CONTACT FOR REAGENT AND RESOURCE SHARING
- EXPERIMENTAL MODEL AND SUBJECT DETAILS
- METHOD DETAILS
  - Preparation of pICL
  - *Xenopus* Egg Extracts and DNA Replication
  - Antibodies and Immunodepletions
  - Nascent-Strand Analysis
  - Error-Free Repair Assay
  - Strand-Specific Southern Blot
  - Replication-Dependent Unhooking Assay
  - Plasmid Pull-Down
  - Purification of Recombinant *Xenopus* FANCI-FANCD2 Complex and NEIL3
  - NEIL3 Glycosylase Assay
- QUANTIFICATION AND STATISTICAL ANALYSIS

SUPPLEMENTAL INFORMATION

Supplemental Information includes seven figures and one table and can be found with this article online at http://dx.doi.org/10.1016/j.cell.2016.09.008.

AUTHOR CONTRIBUTIONS

J.Z. first discovered incision-independent unhooking and characterized psoralen-ICL repair. D.R.S. characterized AP-ICL repair and identified NEIL3 as the ICL glycosylase. M.B. performed the experiments in Figures 2C–2F. A.C.D. supplied 2′-fluoroarabino-dT (FdT) and consulted on data interpretation. J.C.W., J.Z., and D.R.S. designed experiments, analyzed the data, and wrote the paper.

ACKNOWLEDGMENTS

We thank James Dewar and Markus Räschle for sharing unpublished mass spectrometry results, Martin Cohn and Anna Motnenko for the protocol of psoralen-ICL preparation, Markus Räschle for feedback on the manuscript, and members of the J.C.W. lab for discussions. This work was supported by a Jane Coffin Childs postdoctoral fellowship to D.R.S., a Human Frontiers Science Program long-term fellowship (LT000773/2010-L) and a European Molecular Biology Organization long-term fellowship (ALTF 742-2009) to M.B., NIH grants HL98316 and GM62267 to J.C.W, and NIH grant GM072711 to A.C.D. J.C.W is an investigator of the Howard Hughes Medical Institute.

Received: March 4, 2016
Revised: July 28, 2016
Accepted: September 2, 2016
Published: September 29, 2016

REFERENCES

Abramoff, M.D., Magalhaes, P.J., and Ram, S.J. (2004). Image processing with imageJ. Biophoton. Int. *11*, 36–42.

Alt, A., Lammens, K., Chiocchini, C., Lammens, A., Pieck, J.C., Kuch, D., Hopfner, K.P., and Carell, T. (2007). Bypass of DNA lesions generated during anticancer treatment with cisplatin by DNA polymerase eta. Science *318*, 967–970.

Brooks, S.C., Adhikary, S., Rubinson, E.H., and Eichman, B.F. (2013). Recent advances in the structural mechanisms of DNA glycosylases. Biochim. Biophys. Acta *1834*, 247–271.

Budzowska, M., Graham, T.G., Sobeck, A., Waga, S., and Walter, J.C. (2015). Regulation of the Rev1-pol ζ complex during bypass of a DNA interstrand cross-link. EMBO J. *34*, 1971–1985.

Cimino, G.D., Shi, Y.B., and Hearst, J.E. (1986). Wavelength dependence for the photoreversal of a psoralen-DNA cross-link. Biochemistry *25*, 3013–3020.

Clauson, C., Schärer, O.D., and Niedernhofer, L. (2013). Advances in understanding the complex mechanisms of DNA interstrand cross-link repair. Cold Spring Harb. Perspect. Biol. *5*, a012732.

Couvé, S., Macé-Aimé, G., Rosselli, F., and Saparbaev, M.K. (2009). The human oxidative DNA glycosylase NEIL1 excises psoralen-induced interstrand DNA cross-links in a three-stranded DNA structure. J. Biol. Chem. *284*, 11963–11970.

Deans, A.J., and West, S.C. (2009). FANCM connects the genome instability disorders Bloom's syndrome and fanconi anemia. Mol. Cell *36*, 943–953.

Dewar, J.M., Budzowska, M., and Walter, J.C. (2015). The mechanism of DNA replication termination in vertebrates. Nature *525*, 345–350.

Duxin, J.P., and Walter, J.C. (2015). What is the DNA repair defect underlying Fanconi anemia? Curr. Opin. Cell Biol. *37*, 49–60.

Duxin, J.P., Dewar, J.M., Yardimci, H., and Walter, J.C. (2014). Repair of a DNA-protein crosslink by replication-coupled proteolysis. Cell *159*, 346–357.

Enoiu, M., Ho, T.V., Long, D.T., Walter, J.C., and Schärer, O.D. (2012). Construction of plasmids containing site-specific DNA interstrand cross-links for biochemical and cell biological studies. Methods Mol. Biol. *920*, 203–219.

Fu, Y.V., Yardimci, H., Long, D.T., Ho, T.V., Guainazzi, A., Bermudez, V.P., Hurwitz, J., van Oijen, A., Schärer, O.D., and Walter, J.C. (2011). Selective bypass of a lagging strand roadblock by the eukaryotic replicative DNA helicase. Cell *146*, 931–941.

Garaycoechea, J.I., Crossan, G.P., Langevin, F., Daly, M., Arends, M.J., and Patel, K.J. (2012). Genotoxic consequences of endogenous aldehydes on mouse haematopoietic stem cell function. Nature *489*, 571–575.

Guainazzi, A., Campbell, A.J., Angelov, T., Simmerling, C., and Schärer, O.D. (2010). Synthesis and molecular modeling of a nitrogen mustard DNA interstrand crosslink. Chemistry *16*, 12100–12103.

Hildrestrand, G.A., Neurauter, C.G., Diep, D.B., Castellanos, C.G., Krauss, S., Bjørås, M., and Luna, L. (2009). Expression patterns of Neil3 during embryonic brain development and neoplasia. BMC Neurosci. *10*, 45.

Houghtaling, S., Newell, A., Akkari, Y., Taniguchi, T., Olson, S., and Grompe, M. (2005). Fancd2 functions in a double strand break repair pathway that is distinct from non-homologous end joining. Hum. Mol. Genet. *14*, 3027–3033.

Joenje, H., and Patel, K.J. (2001). The emerging genetic and molecular basis of Fanconi anaemia. Nat. Rev. Genet. *2*, 446–457.

Klein Douwel, D., Boonen, R.A., Long, D.T., Szypowska, A.A., Räschle, M., Walter, J.C., and Knipscheer, P. (2014). XPF-ERCC1 acts in Unhooking DNA interstrand crosslinks in cooperation with FANCD2 and FANCP/SLX4. Mol. Cell *54*, 460–471.

Knipscheer, P., Räschle, M., Smogorzewska, A., Enoiu, M., Ho, T.V., Schärer, O.D., Elledge, S.J., and Walter, J.C. (2009). The Fanconi anemia pathway promotes replication-dependent DNA interstrand cross-link repair. Science *326*, 1698–1701.

Kottemann, M.C., and Smogorzewska, A. (2013). Fanconi anaemia and the repair of Watson and Crick DNA crosslinks. Nature *493*, 356–363.

Krokeide, S.Z., Laerdahl, J.K., Salah, M., Luna, L., Cederkvist, F.H., Fleming, A.M., Burrows, C.J., Dalhus, B., and Bjørås, M. (2013). Human NEIL3 is mainly a monofunctional DNA glycosylase removing spiroimindiohydantoin and guanidinohydantoin. DNA Repair (Amst.) *12*, 1159–1164.

Langevin, F., Crossan, G.P., Rosado, I.V., Arends, M.J., and Patel, K.J. (2011). Fancd2 counteracts the toxic effects of naturally produced aldehydes in mice. Nature *475*, 53–58.

Lebofsky, R., Takahashi, T., and Walter, J.C. (2009). DNA replication in nucleus-free Xenopus egg extracts. Methods Mol. Biol. *521*, 229–252.

Lee, K.Y., Yang, I., Park, J.E., Baek, O.R., Chung, K.Y., and Koo, H.S. (2007). Developmental stage- and DNA damage-specific functions of C. elegans FANCD2. Biochem. Biophys. Res. Commun. *352*, 479–485.

Liao, S., Matsumoto, Y., and Yan, H. (2007). Biochemical reconstitution of abasic DNA lesion replication in Xenopus extracts. Nucleic Acids Res. *35*, 5422–5429.

Liu, M., Bandaru, V., Bond, J.P., Jaruga, P., Zhao, X., Christov, P.P., Burrows, C.J., Rizzo, C.J., Dizdaroglu, M., and Wallace, S.S. (2010). The mouse ortholog of NEIL3 is a functional DNA glycosylase in vitro and in vivo. Proc. Natl. Acad. Sci. USA *107*, 4925–4930.

Liu, M., Bandaru, V., Holmes, A., Averill, A.M., Cannan, W., and Wallace, S.S. (2012). Expression and purification of active mouse and human NEIL3 proteins. Protein Expr. Purif. *84*, 130–139.

Liu, M., Doublié, S., and Wallace, S.S. (2013a). Neil3, the final frontier for the DNA glycosylases that recognize oxidative damage. Mutat. Res. *743-744*, 4–11.

Liu, M., Imamura, K., Averill, A.M., Wallace, S.S., and Doublié, S. (2013b). Structural characterization of a mouse ortholog of human NEIL3 with a marked preference for single-stranded DNA. Structure *21*, 247–256.

Long, D.T., Räschle, M., Joukov, V., and Walter, J.C. (2011). Mechanism of RAD51-dependent DNA interstrand cross-link repair. Science *333*, 84–87.

Long, D.T., Joukov, V., Budzowska, M., and Walter, J.C. (2014). BRCA1 promotes unloading of the CMG helicase from a stalled DNA replication fork. Mol. Cell *56*, 174–185.

Magnaghi, P., D'Alessio, R., Valsasina, B., Avanzi, N., Rizzi, S., Asa, D., Gasparri, F., Cozzi, L., Cucchi, U., Orrenius, C., et al. (2013). Covalent and allosteric inhibitors of the ATPase VCP/p97 induce cancer cell death. Nat. Chem. Biol. *9*, 548–556.

Maiti, A., Morgan, M.T., and Drohat, A.C. (2009). Role of two strictly conserved residues in nucleotide flipping and N-glycosylic bond cleavage by human thymine DNA glycosylase. J. Biol. Chem. *284*, 36680–36688.

Maric, M., Maculins, T., De Piccoli, G., and Labib, K. (2014). Cdc48 and a ubiquitin ligase drive disassembly of the CMG helicase at the end of DNA replication. Science *346*, 1253596.

Moreno, S.P., Bailey, R., Campion, N., Herron, S., and Gambus, A. (2014). Polyubiquitylation drives replisome disassembly at the termination of DNA replication. Science *346*, 477–481.

Mullins, E.A., Shi, R., Parsons, Z.D., Yuen, P.K., David, S.S., Igarashi, Y., and Eichman, B.F. (2015). The DNA glycosylase AlkD uses a non-base-flipping mechanism to excise bulky lesions. Nature *527*, 254–258.

Nakamura, J., and Swenberg, J.A. (1999). Endogenous apurinic/apyrimidinic sites in genomic DNA of mammalian tissues. Cancer Res. *59*, 2522–2526.

Neurauter, C.G., Luna, L., and Bjørås, M. (2012). Release from quiescence stimulates the expression of human NEIL3 under the control of the Ras dependent ERK-MAP kinase pathway. DNA Repair (Amst.) *11*, 401–409.

Pontel, L.B., Rosado, I.V., Burgos-Barragan, G., Garaycoechea, J.I., Yu, R., Arends, M.J., Chandrasekaran, G., Broecker, V., Wei, W., Liu, L., et al. (2015). Endogenous Formaldehyde Is a Hematopoietic Stem Cell Genotoxin and Metabolic Carcinogen. Mol. Cell *60*, 177–188.

Price, N.E., Johnson, K.M., Wang, J., Fekry, M.I., Wang, Y., and Gates, K.S. (2014). Interstrand DNA-DNA cross-link formation between adenine residues and abasic sites in duplex DNA. J. Am. Chem. Soc. *136*, 3483–3490.

Price, N.E., Catalano, M.J., Liu, S., Wang, Y., and Gates, K.S. (2015). Chemical and structural characterization of interstrand cross-links formed between abasic sites and adenine residues in duplex DNA. Nucleic Acids Res. *43*, 3434–3441.

Räschle, M., Knipscheer, P., Enoiu, M., Angelov, T., Sun, J., Griffith, J.D., Ellenberger, T.E., Schärer, O.D., and Walter, J.C. (2008). Mechanism of replication-coupled DNA interstrand crosslink repair. Cell *134*, 969–980.

Räschle, M., Smeenk, G., Hansen, R.K., Temu, T., Oka, Y., Hein, M.Y., Nagaraj, N., Long, D.T., Walter, J.C., Hofmann, K., et al. (2015). DNA repair. Proteomics reveals dynamic assembly of repair complexes during bypass of DNA cross-links. Science *348*, 1253671.

Rolseth, V., Krokeide, S.Z., Kunke, D., Neurauter, C.G., Suganthan, R., Sejersted, Y., Hildrestrand, G.A., Bjørås, M., and Luna, L. (2013). Loss of Neil3, the major DNA glycosylase activity for removal of hydantoins in single stranded DNA, reduces cellular proliferation and sensitizes cells to genotoxic stress. Biochim. Biophys. Acta *1833*, 1157–1164.

Rothfuss, A., and Grompe, M. (2004). Repair kinetics of genomic interstrand DNA cross-links: evidence for DNA double-strand break-dependent activation of the Fanconi anemia/BRCA pathway. Mol. Cell. Biol. *24*, 123–134.

Sejersted, Y., Hildrestrand, G.A., Kunke, D., Rolseth, V., Krokeide, S.Z., Neurauter, C.G., Suganthan, R., Atneosen-Åsegg, M., Fleming, A.M., Saugstad, O.D., et al. (2011). Endonuclease VIII-like 3 (Neil3) DNA glycosylase promotes neurogenesis induced by hypoxia-ischemia. Proc. Natl. Acad. Sci. USA *108*, 18802–18807.

Taniguchi, T., Garcia-Higuera, I., Xu, B., Andreassen, P.R., Gregory, R.C., Kim, S.T., Lane, W.S., Kastan, M.B., and D'Andrea, A.D. (2002). Convergence of the fanconi anemia and ataxia telangiectasia signaling pathways. Cell *109*, 459–472.

Torisu, K., Tsuchimoto, D., Ohnishi, Y., and Nakabeppu, Y. (2005). Hematopoietic tissue-specific expression of mouse Neil3 for endonuclease VIII-like protein. J. Biochem. *138*, 763–772.

Walter, J., and Newport, J. (2000). Initiation of eukaryotic DNA replication: origin unwinding and sequential chromatin association of Cdc45, RPA, and DNA polymerase alpha. Mol. Cell *5*, 617–627.

Wang, S., Liu, K., Xiao, L., Yang, L., Li, H., Zhang, F., Lei, L., Li, S., Feng, X., Li, A., and He, J. (2016). Characterization of a novel DNA glycosylase from S. sahachiroi involved in the reduction and repair of azinomycin B induced DNA damage. Nucleic Acids Res. *44*, 187–197.

Williams, H.L., Gottesman, M.E., and Gautier, J. (2013). The differences between ICL repair during and outside of S phase. Trends Biochem. Sci. *38*, 386–393.

Zhang, J., and Walter, J.C. (2014). Mechanism and regulation of incisions during DNA interstrand cross-link repair. DNA Repair (Amst.) *19*, 135–142.

Zhang, J., Dewar, J.M., Budzowska, M., Motnenko, A., Cohn, M.A., and Walter, J.C. (2015). DNA interstrand cross-link repair requires replication-fork convergence. Nat. Struct. Mol. Biol. *22*, 242–247.

Please cite this article in press as: Semlow et al., Replication-Dependent Unhooking of DNA Interstrand Cross-Links by the NEIL3 Glycosylase, Cell (2016), http://dx.doi.org/10.1016/j.cell.2016.09.008

STAR★METHODS

KEY RESOURCES TABLE

REAGENT or RESOURCE	SOURCE	IDENTIFIER
Antibodies		
Rabbit polyclonal anti-FANCD2	Knipscheer et al., 2009	Rabbit 20019
Rabbit polyclonal anti-FANCI	Duxin et al., 2014	Rabbits 26651 and 26864
Rabbit polyclonal anti-CDC45	Walter and Newport, 2000	Rabbit 534
Rabbit polyclonal anti-MCM6	New England Peptide	Project #2926
Rabbit polyclonal anti-H3	Cell Signaling Technology	Cat #9715
Rabbit polyclonal anti-REV1	Budzowska et al., 2015	Rabbits 714 and 1010
Rabbit polyclonal anti-NEIL3	New England Peptide; this study	Project #3470
Rabbit polyclonal anti-NEIL3	Abgent; this study	Rabbit 57141
Chemicals, Peptides, and Recombinant Proteins		
Recombinant *Xenopus laevis* NEIL3-FLAG	this study	N/A
Recombinant *Xenopus laevis* NEIL3-FLAG K60A	this study	N/A
Recombinant *Xenopus laevis* FANCI-FANCD2	Knipscheer et al., 2009	N/A
2′-fluoroarabino-dT (FdT)	LINK Technologies	N/A
NMS-873	Sigma	Cat #SML1128
Trioxsalen	Sigma	Cat #T6137
Critical Commercial Assays		
Thermo Sequenase Cycle Sequencing Kit	USB	Cat#785001KT
Random Primed DNA Labeling Kit	Roche	Cat#11004760001
Bac to Bac Expression System	Thermo Fisher Scientific	Cat#10359016
Experimental Models: Cell Lines		
Sf9 insect cells	Thermo Fisher Scientific	Cat#B82501
Experimental Models: Organisms/Strains		
Xenopus laevis	Nasco	Cat #LM0053MX
Recombinant DNA		
pICL-*lacO*^{Pt}	Zhang et al., 2015	N/A
pICL-*lacO*^{Pso}	Zhang et al., 2015	N/A
pICL-*lacO*^{AP}	This study	N/A
pICL-*lacO*$^{AP\text{-}reverse}$	This study	N/A
pCtrl-*lacO*	Dewar et al., 2015	N/A
pICL^{Pt}	Räschle et al., 2008	N/A
pICL^{AP}	This study	N/A
pCtrl	Räschle et al., 2008	N/A
pFastBac1-NEIL3-FLAG	This study	N/A
pFastBac1-NEIL3K60A-FLAG	This study	N/A
Sequence-Based Reagents		
See Table S1 for sequences of primers and oligonucleotides used in the preparation of pICLs and AP-ICL unhooking substrates	This study	N/A
Software and Algorithms		
ImageJ	Abramoff et al., 2004	N/A

CONTACT FOR REAGENT AND RESOURCE SHARING

Further information and requests for reagents may be directed to, and will be fulfilled by, the Lead Contact, Johannes Walter, at johannes_walter@hms.harvard.edu.

EXPERIMENTAL MODEL AND SUBJECT DETAILS

Egg extracts were prepared using *Xenopus laevis* (Nasco Cat #LM0053MX). All experiments involving animals were approved by the Harvard Medical Area Institutional Animal Care and Used Committee and conform to relevant regulatory standards.

METHOD DETAILS

All experiments were performed at least twice, and a representative result is shown.

Preparation of pICL

The preparation of pICL was performed as previously described (note that the psoralen-ICL plasmids used in this paper contain an array of 48 lacO repeats in the vector backbone, as do AP-ICL plasmids, except those used in Figures 5, S5, and 6; Enoiu et al., 2012; Zhang et al., 2015). Briefly, the parental plasmid was digested with BbsI. The purified, crosslinked duplex oligonucleotide was then ligated into the tandem BbsI sites of the corresponding backbone plasmid. To make psoralen-ICL plasmids, complementary primers containing only one thymidine (or 2′-fluoroarabino-dT (FdT) for pICL$^{FdT\text{-}Pso}$) were annealed in annealing buffer (100 mM potassium acetate, 30 mM HEPES-KOH [pH 7.4], and 2 mM magnesium acetate) at a concentration of 50 μM each. DNA-trioxsalen (referred as psoralen in the main text) crosslinking was carried out using 2.6 μM annealed DNA in crosslinking buffer (10 mM Tris [pH 7.5], 1 mM EDTA, 50 mM NaCl) and 87.6 μM trioxsalen (Sigma). The reaction was exposed to 365 nm UVA light for six periods of 15 min each, at a power of 4 mW/cm^2. After every cycle, fresh trioxsalen was added to 87.6 μM. Cross-linked DNA was purified from a 20% polyacrylamide, 8 M urea gel. FdT was synthesized by LINK technology (Maiti et al., 2009). DNA oligonucleotides containing FdT were synthesized and purified at the Keck Foundation Biotechnology Resource Laboratory at Yale University.

To make AP-ICL plasmids, an oligonucleotide containing a single deoxyuracil (IDT) was crosslinked to its complement essentially as described (Price et al., 2014). Briefly, the oligonucleotides were annealed in 30 mM HEPES-KOH (pH 7.0), 100 mM NaCl by heating to 95°C for 5 min and cooling at 1°C/min to 18°C. The annealed duplex was then treated with uracil gylcosylase (NEB) in UDG buffer (20 mM Tris-HCl, 10 mM DTT, 10 mM EDTA [pH 8.0]) for 2 hr at 37°C followed by extraction with phenol:chloroform:isoamyl alcohol (25:24:1; pH 8) and ethanol precipitation. The duplex was then dissolved in 50 mM HEPES-KOH (pH 7.0), 100 mM NaCl and incubated at 37°C for 120 hr to allow cross-link formation. Cross-linked DNA was purified from a 20% polyacrylamide, 8 M urea gel.

To confirm the presence of the cross-links within the ligated plasmids, 150 ng pICL was digested with 5 U NotI (NEB) in 1x NEB buffer 3.1 for 120 min at 37°C. The resulting digestion fragments were then treated with 5 U calf intestinal phosphatase (NEB) for 60 min at 37°C followed by extraction with phenol:chloroform:isoamyl alcohol (25:24:1; pH 8) and ethanol precipitation. The fragments were then 5′ end radiolabeled with [γ-^{32}P]dATP and T4 PNK (NEB), separated on a 15% polyacrylamide (19:1), 8 M urea, 1x TBE gel, and visualized by autoradiography.

Psoralen cross-linked duplexes (with the cross-link between the two highlighted Ts: thymidine for a normal psoralen-ICL, 2′-fluoroarabino-dT for a FdT-Psoralen-ICL):

5′-CCCCGGGGC**T**AGCC-3′
5′-GCACGGC**T**AGCCCC-3′

Abasic site cross-linked oligo duplexes (the cross-link occurs between the positions in bold; the ICL was generated in two orientations [AP site on top strand versus AP site on bottom strand] by swapping the underlined overhangs that are complementary to the pICL backbone):

5′-<u>CCCT</u>CTTCCGCTC**dU**TCTTTC-3′
5′-<u>GCAC</u>GAAAG**A**AGAGCGGAAG-3′

Xenopus Egg Extracts and DNA Replication

Xenopus egg extracts were prepared as described (Lebofsky et al., 2009). For DNA replication, plasmids were first incubated in a high-speed supernatant (HSS) of egg cytoplasm (final concentration of 7.5 ng DNA/μL extract) for 20-30 min at room temperature to license the DNA, followed by the addition of two volumes of nucleoplasmic egg extract (NPE) to initiate replication. Where indicated, NPE was supplemented with ~310 nM recombinant *Xenopus* FANCI-D2 complex or the indicated amount of recombinant *Xenopus* NEIL3. In all figures, the 0 min time point refers to the time of NPE addition. For DNA labeling, reactions were supplemented with [α-^{32}P]dATP, which is incorporated into nascent strands during replication. Where indicated, NMS-873 P97 inhibitor (Sigma) was used at a concentration of 200 μM in NPE. For replication assays without digestion, replication was stopped by adding 0.5 μl of each reaction to 10 μl of replication stop solution A (5% SDS, 80 mM Tris pH 8.0, 0.13% phosphoric acid, 10% Ficoll) supplemented with 1 μl Proteinase K (20 mg/ml) (Roche). Samples were incubated for 1 hr at 37°C prior to separation by 0.8% native agarose gel electrophoresis. DNA samples were then detected using a phosphorimager (Lebofsky et al., 2009). For all other applications, replication reactions were stopped in 10 volumes of 50 mM Tris (pH 7.5), 0.5% SDS, 25 mM EDTA, and replication intermediates were purified as previously described (Räschle et al., 2008). Where indicated, replication intermediates were digested with 0.08 U/μL HincII (NEB) and/or 0.08 U/μL APE1 (NEB).

Antibodies and Immunodepletions

Immunodepletions using antibodies against FANCD2 (Rabbit 20019; Knipscheer et al., 2009), FANCI (Rabbit 26864; Duxin et al., 2014), and REV1 (Rabbits 714 and 1010; Budzowska et al., 2015) were performed as described previously (Budzowska et al., 2015). Briefly, protein A Sepharose Fast Flow beads (GE Healthcare) were incubated with antibodies overnight. Two rounds of FANCI-D2 co-depletion were performed at room temperature for 20 min each and three rounds of REV1 depletion were performed at 4 degrees for 1 hr each. For NEIL3 immunodepletion, 2.5 volumes of affinity purified antibodies against NEIL3 (1 mg/mL; New England Peptide project #3470) were incubated with 1 volume Sepharose Fast Flow beads overnight at 4°C. Three rounds of NEIL3 depletion were then performed by incubating five volumes of egg extract with 1 volume antibody-bound beads for 1 hr at 4°C. Western blots were probed using antibodies against REV1 (Rabbit 1010), FANCD2 (Rabbit 20019), FANCI (Rabbit 26651), MCM6 (New England Peptide project #2926), CDC45 (Rabbit 534; Walter and Newport, 2000), Histone H3 (Cell Signaling Technology #9715), and NEIL3 (New England Peptide project #3470 or Rb57141).

Nascent-Strand Analysis

Nascent strand analysis was performed as described (Räschle et al., 2008). Briefly, pICL plasmids were replicated in the presence of [α-^{32}P]dATP as described above, and purified replication products were digested with AflIII or AflIII and EcoRI, as indicated, followed by addition of 0.5 volumes Gel loading Buffer II (Life Technologies). Radiolabeled nascent strands were then separated on a 7% denaturing polyacrylamide gel, transferred to filter paper, dried, and visualized by autoradiography. Sequencing gel markers (not shown) were generated using the Thermo Sequenase Cycle Sequencing kit (USB Corporation) with a primer (5′-CATGTTTTACTAGC CAGATTTTTCCTCCTCTCCTG-3′) that anneals to pICL 149 nucleotides upstream of the cross-link.

Error-Free Repair Assay

The error-free repair assay was performed as described (Räschle et al., 2008). Briefly, pICL^{Pso} or pICL^{AP} was replicated in the presence or absence of geminin (400 nM in HSS). A 1.2 kb ApaLI or 0.9 kb HindIII pCtrl digestion fragment was added before extraction as the loading control. The replication products were harvested and digested with HincII/NheI (for pICL^{Pso}) or HincII/SapI (for pICL^{AP}), and separated on a 1% agarose gel. Southern blotting was subsequently performed. DNA was fragmented in 0.25 N HCl for 10 min and then transferred (1.5 M NaCl, 0.4 M NaOH transfer buffer) onto a Hybond-N+ membrane (Amersham) by capillary action overnight. After transfer, the membrane was washed in 4X SSC for 5 min, and UV irradiated to cross-link the DNA to the membrane. Prehybridization was performed with 25 ml of hybridization buffer (4X SSC, 2% SDS, 1X Blocking reagent (Roche), 0.1 mg/ml Salmon sperm DNA (Life Technologies) for 30 min at 45°C. Hybridization was carried out overnight with 25 μl of probe prepared with Roche random labeling kit (Roche) using pCtrl as a template. After overnight hybridization, the membrane was washed 4 times with 0.5X SSC, 0.25% SDS for 15 min at 45°C. The dried membrane was exposed to a phosphorimager screen, and the repair products were quantified.

Strand-Specific Southern Blot

Strand-specific Southern blot was performed as previously described (Räschle et al., 2008; Zhang et al., 2015). Briefly, AflIII and AseI digested replication intermediates were separated on a 7% polyacrylamide gel and transferred to a Hybond-N+ membrane (Amersham). After transfer, the membrane was rinsed in 4X SSC for 5 min, and UV irradiated to crosslink the DNA to the membrane. The membrane was then pre-hybridized with 25 ml Ultrahyb buffer (Ambion) for at least 3 hr at 42°C. Strand-specific probes generated by a PCR based primer extension reaction (Räschle et al., 2008) were added to the hybridization buffer and incubated with the membrane at 42°C overnight. The membrane was washed 2 times with 2X SSC, 0.1% SDS for 5 min at 42°C, dried, and exposed to a phosphorimager screen. In Figure 2J, the original images were converted into a log scale for display by applying the function f(p) = log (p)*255/log (255) to each pixel (p) in the images.

Replication-Dependent Unhooking Assay

pICL^{Pso} or pICL^{AP} was replicated in the presence or absence of geminin (400 nM in HSS). The replication products were isolated, digested with HincII, and separated on an alkaline 0.9% agarose gel (50 mM NaOH, 1 mM EDTA [pH 8.0]). Southern blotting was subsequently performed. DNA was fragmented in 0.25 N HCl for 10 min and transferred (1.5 M NaCl, 0.4 M NaOH transfer buffer) to a Hybond-N+ membrane (Amersham) by capillary action overnight. After transfer, the membrane was washed in 4X SSC for 5 min, and UV irradiated at 120,000 μJ/cm^2 to cross-link the DNA to the membrane. Pre-hybridization was performed in 20 ml of Ultrahyb buffer (Ambion) for 18 hr at 42°C. Hybridization was carried out overnight at 42°C with 25 μl of probe prepared with Roche Random Primed DNA Labeling Kit (Roche) using pCtrl as a template. The membrane was then washed twice with 1X SSC, 0.6% SDS for 15 min at 45°C and twice with 0.1x SSC, 0.6% SDS for 15 min at 65°C and then visualized by autoradiography.

Plasmid Pull-Down

The plasmid pull down assay was performed as described (Budzowska et al., 2015). Briefly, streptavidin-coupled magnetic beads (Invitrogen; 6 μl per pull-down) were washed three times with 50 mM Tris (pH 7.5), 150 mM NaCl, 1 mM EDTA pH 8, 0.02% Tween-20. Biotinylated LacI was added to the beads (12 pmol per 6 μl beads) and incubated at room temperature for 40 min. The beads were then washed four times with 10 mM HEPES (pH 7.7), 50 mM KCl, 2.5 mM MgCl2, 250 mM sucrose, 0.25 mg/ml BSA, 0.02% Tween-20

and resuspended in 40 μl of the same buffer. The bead suspension was stored on ice until needed. At the indicated times, 8 μl samples of the replication reaction were withdrawn and gently mixed with LacI-coated streptavidin Dynabeads. The suspension was immediately placed on a rotating wheel and incubated for 30 min at 4°C. The beads were washed three times with 10 mM HEPES (pH 7.7), 50 mM KCl, 2.5 mM $MgCl_2$, 0.25 mg/ml BSA, 0.03% Tween-20. All residual buffer was removed, and the beads were resuspended in 40 μl of 2X Laemmli sample buffer. Equal volumes of the protein samples were blotted with the indicated antibodies.

Purification of Recombinant *Xenopus* FANCI-FANCD2 Complex and NEIL3

Xenopus FANCI-FANCD2 complex was purified from baculovirus infected Sf9 cells as described previously (Knipscheer et al., 2009). NEIL3 was PCR amplified from a cDNA library prepared from *Xenopus laevis* eggs (a gift from T.G.W. Graham) using primers A and B below. The NEIL3 cDNA was then re-amplified using primers C and D to introduce a C-terminal FLAG epitope tag, digested with EcoRI and XhoI, and ligated into a similarly digested pFastBac1 vector (Thermo Fisher Scientific). The NEIL3-K60A mutation was introduced by Quikchange mutagenesis using primers E and F and confirmed by Sanger sequencing. Baculoviruses expressing NEIL3 were then prepared using the Bac-to-Bac system (Thermo Fisher Scientific) according to the manufacturer's protocols. NEIL3 protein was expressed in 250 ml suspension cultures of Sf9 insect cells (Thermo Fisher Scientific) by infection with baculovirus expressing NEIL3-FLAG for 72 hr. Sf9 cells were collected and suspended in 10 ml lysis buffer (50 mM Tris-HCl [pH 7.5], 300 mM NaCl, 10% glycerol, 1x Roche EDTA-free Complete protease inhibitor cocktail, 0.5 mM PMSF, 0.2% Triton X-100). Cells were lysed by sonication and the soluble fraction was collected by spinning the lysate at 25,000 rpm in a Beckman SW41 rotor for 1 hr. The soluble lysate was incubated with 200 μl anti-FLAG M2 affinity resin (Sigma) for 90 min at 4°C. The resin was washed once with 10 ml lysis buffer, twice with wash buffer (50 mM Tris-HCl [pH 7.5], 300 mM NaCl, 10% glycerol, 0.2% Triton X-100), and three times with buffer A (50 mM Tris-HCl [pH 7.5], 300 mM NaCl, 10% glycerol). NEIL3-FLAG protein was eluted from the resin with buffer A containing 100 μg/ml 3x FLAG peptide (Sigma). Elution fractions containing NEIL3-FLAG protein were pooled and dialyzed against 50 mM HEPES-KOH (pH 7.0), 300 mM NaCl, 1 mM DTT, 20% glycerol at 4°C for 12 hr and then dialyzed against 50 mM HEPES-KOH (pH 7.0), 150 mM NaCl, 1 mM DTT, 15% glycerol at 4°C for 3 hr. Aliquots of protein (~0.15 mg/ml) were stored at −80°C.

Primer A: CAATTATGGTGGAGGGTCCGGG
Primer B: CTGTTTCACGTCTACTCTGTTTTTGCCC
Primer C: GCGCGCGGAATTCACCATGGTGGAGGGTCCGGGCTG
Primer D: CCAGCCCTCGAGCGTCTACTTGTCGTCATCGTCTTTGTAGTCACATGCCCAGTGCTCTTC
Primer E: GCTACGCTGGAGTGGAAACGCTGGGAGCGGAGCTTTTTATAT
Primer F: ATATAAAAAGCTCCGCTCCCAGCGTTTCCACTCCAGCGTAGC

NEIL3 Glycosylase Assay

AP-ICLs between complementary DNA or DNA/RNA chimeric oligonucleotides (IDT) were prepared and gel purified as described above. AP-ICLs were digested with 0.16 mg/ml RNase A (Sigma) and 0.2 U/μL RNase H (NEB) in 50 mM Tris-HCl (pH 8.3), 75 mM KCl, 3 mM $MgCl_2$, 10 mM DTT at 37°C for 120 min and then purified to remove RNA. To monitor unhooking of AP-ICLs, 2.5 nM 5′ radiolabeled cross-linked substrate was incubated with 20 nM recombinant NEIL3 in 20 mM HEPES-KOH (pH 7.0), 50 mM NaCl, 1 mM DTT, 0.1 mg/ml BSA for 60 min at 37°C (Liu et al., 2010). Reactions were quenched with 1 volume of 2x formamide buffer (86% formamide, 2x TBE, 20 mM EDTA [pH 8.0]), separated on a denaturing polyacrylamide and visualized by autoradiography.

Sequences of oligonucleotides for NEIL3 glycosylase assay (positions of cross-links are indicated in bold):

AP-ICL top (DNA): GCCATAGTAAG**A**AGAGCCGAATGC
AP-ICL top (DNA/RNA): rGrCrCrArUrArGrUrArAG**A**ArGrArGrCrCrGrArArUrGrC
AP-ICL bottom (DNA): GCATTCGGCTC**dU**TCTTACTATGGC
AP-ICL bottom (DNA/RNA): rGrCrArUrUrCrGrGrCrUC**dU**TrCrUrUrArCrUrArUrGrGrC

QUANTIFICATION AND STATISTICAL ANALYSIS

Autoradiographs were quantified using ImageJ.

Supplemental Figures

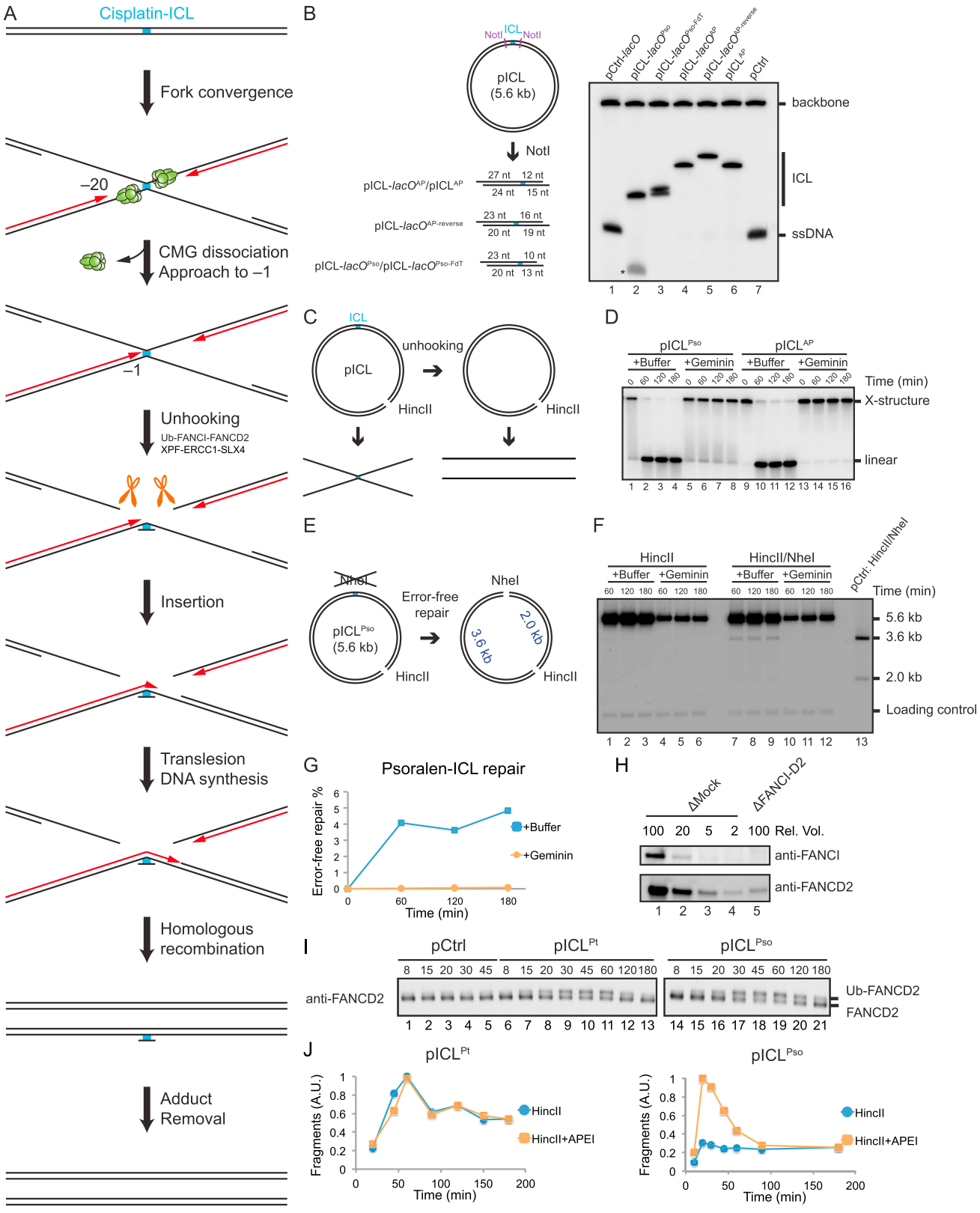

(legend on next page)

Figure S1. Psoralen- and AP-ICLs Are Unhooked in a Replication-Dependent Manner, Related to Figure 1

(A) Model of replication-coupled cisplatin-ICL repair. See main text for details.

(B) Extent of cross-linking for pICLs. ICL-containing plasmids were digested with NotI and the resulting fragments were 5′ end radiolabeled, separated on a denaturing polyacrylamide gel, and visualized by autoradiography. The fraction of plasmid in the cross-linked band versus the ssDNA band plus the cross-linked band was calculated and in each case was found to be at least 97%. For pICL-*lacO*^{Pso}, there was an additional, faster migrating band (*) that likely represents cross-linked species that was not denatured during electrophoresis.

(C) Unhooking assay for pICL^{Pso} and pICL^{AP}. Digestion of pICL^{Pso} and pICL^{AP} generates an X-structure prior to unhooking and linear species subsequent to unhooking.

(D) Replication-dependent unhooking of pICL^{Pso} and pICL^{AP}. pICL^{Pso} and pICL^{AP} were replicated in egg extract in the presence or absence of geminin, as indicated. Repair intermediates were digested with HincII, separated on a denaturing agarose gel, and visualized by Southern blotting. Generation of the unhooked linear species illustrated in (C) was blocked in the absence of DNA replication.

(E) Error-free repair assay for pICL^{Pso}. pICL^{Pso} contains an NheI site that is blocked by the ICL but becomes cleavable after error-free repair. Digestion of repaired plasmids with HincII and NheI generates 3.6 kb and 2.0 kb fragments.

(F) Error-free repair of pICL^{Pso}. pICL^{Pso} was replicated in egg extract in the presence or absence of geminin, as indicated. Repair intermediates were digested with HincII or HincII and NheI, separated on a native agarose gel, and visualized by Southern blotting. A 1.2 kb ApaLI-digested pCtrl fragment was added before DNA extraction as a loading control. 33% of input pCtrl was digested with HincII/Nhe1 and loaded in lane 13.

(G) Quantification of error-free repair efficiency of pICL^{Pso} shown in (F). Efficiency of error-free pICL^{Pso} repair was quantified as the ratio of error-free repair products to total linear species ([3.6 kb + 2.0 kb]/[5.6 kb +3.6 kb + 2.0 kb]).

(H) FANCI-D2 immunodepletion. Mock-depleted and FANCI-D2-depleted NPE was analyzed by Western blotting using FANCI or FANCD2 antibody. A relative volume of 100 corresponds to 0.25 μl NPE.

(I) pICL^{Pso} stimulates FANCD2 ubiquitylation. pCtrl, pICL^{Pt}, or pICL^{Pso} was replicated in egg extract and, at the indicated times, samples of total extract were analyzed by Western blotting using FANCD2 antibody. Samples shown were processed in parallel but analyzed on separate blots. Replication of pCtrl also caused some basal level of FANCD2 ubiquitylation, consistent with earlier observations (Räschle et al., 2008; Taniguchi et al., 2002).

(J) The 3.6 kb and 2.0 kb fragments in Figure 2H were quantified and plotted.

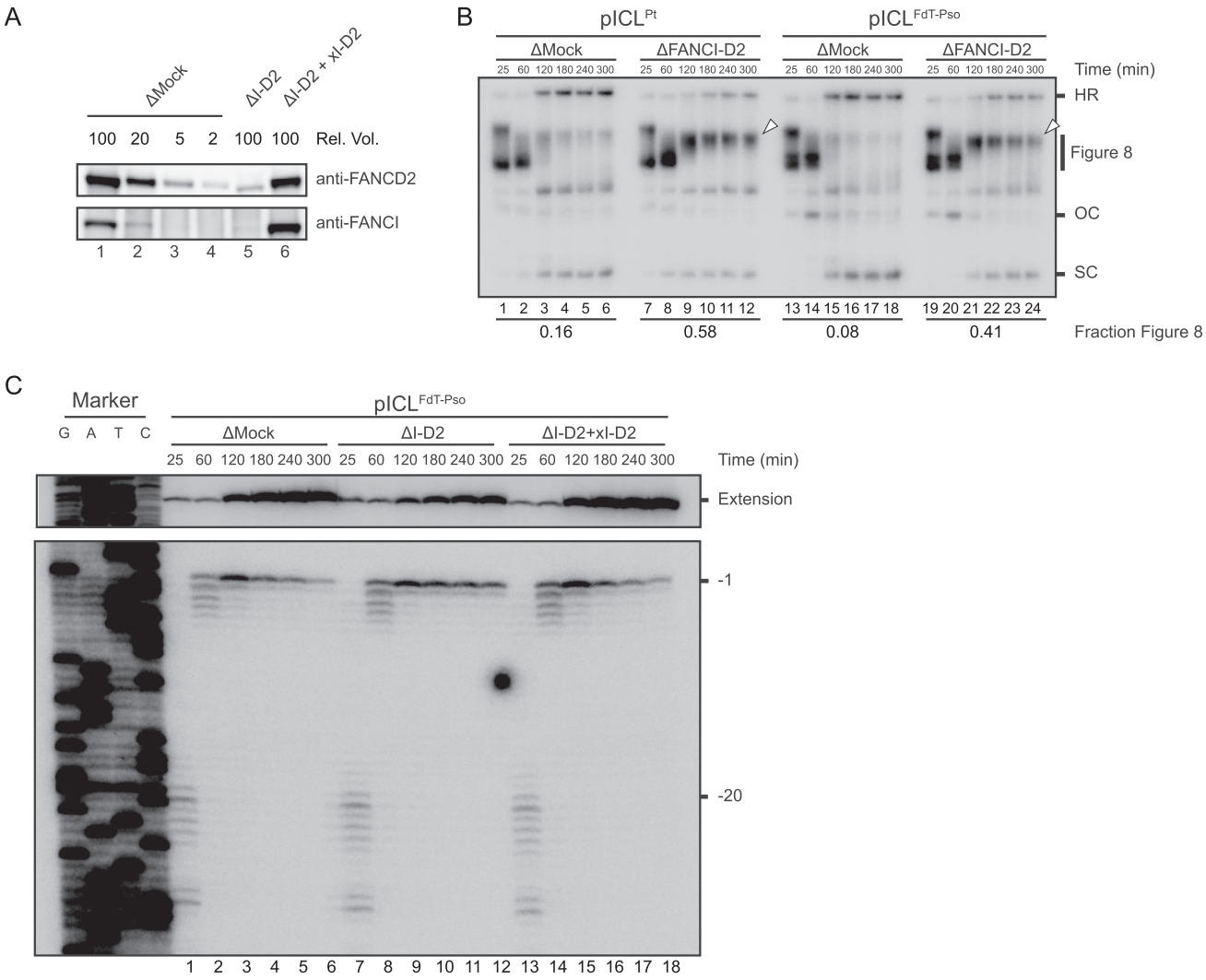

Figure S2. Repair of a 2′FdT-Psoralen-ICL Requires FANCI-FANCD2, Related to Figure 3

(A) FANCI-D2 immunodepletion. Mock-depleted NPE, FANCI-D2-depleted NPE (ΔI-D2), and ΔI-D2 NPE supplemented with xFANCI-D2 (ΔI-D2+xI-D2) were blotted with FANCI or FANCD2 antibody. A relative volume of 100 corresponds to 0.25 μl NPE.

(B) pICL^{Pt} or pICL$^{FdT\text{-}Pso}$ was replicated in mock- or FANCI-D2-depleted egg extracts in the presence of [α-^{32}P]dATP and analyzed as in Figure 1C. White arrowheads, Figure 8 structures that persist in the absence of FANCI-D2. The fraction Figure 8 indicates the proportion of Figure 8 structures relative to total species at 300 min.

(C) pICL$^{FdT\text{-}Pso}$ was replicated in mock-depleted egg extract, FANCI-D2-depleted extract (ΔI-D2), or ΔI-D2 extract supplemented with xFANCI-D2 (ΔI-D2 + xI-D2) in the presence of [α-^{32}P]dATP (Experiment described in Figure 3C). DNA was purified and digested with AflIII and EcoRI before separation on a denaturing polyacrylamide gel.

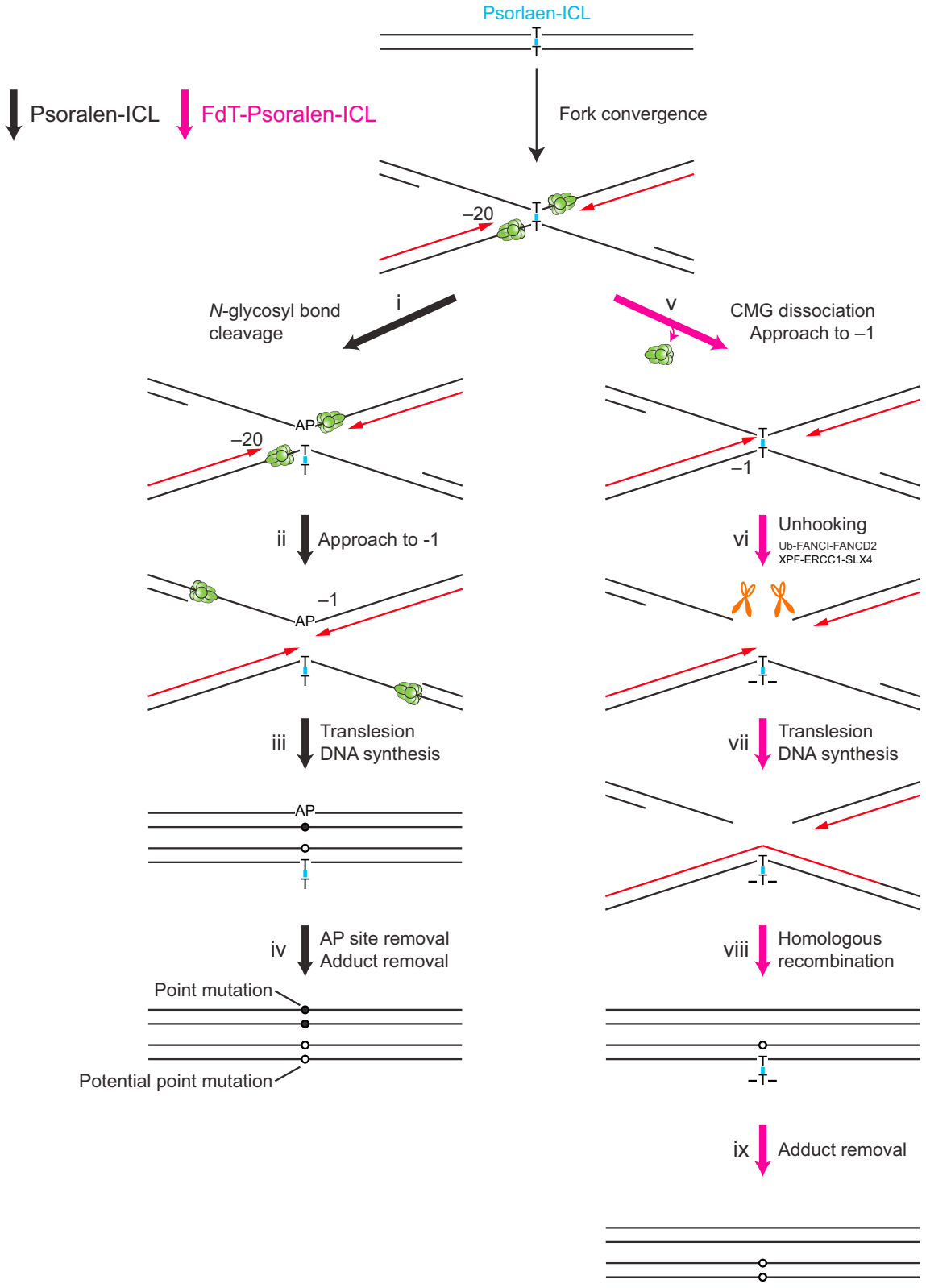

(legend on next page)

Figure S3. Model for Repair of a Psoralen-ICL, Related to Figure 3

Repair of a thymidine-psoralen-ICL (black arrows) or 2′ fluoro-thymidine-psoralen-ICL (pink arrows) by incision-independent (left branch) or incision-dependent (right branch) pathways. See main text for details. Black lines, parental DNA. Red lines, nascent leading strands. Cyan, psoralen-ICL. Green ovals, CMG helicase. Closed circles indicate point mutations that arise due to bypass of an AP site. Open circles indicate potential point mutations that may be introduced due to bypass of a thymidine mono-adduct. Note that although bypass of a guanosine mono-adduct derived from a cisplatin-ICL was previously shown to be largely error-free, it is unknown whether bypass of a thymidine mono-adduct derived from a psoralen-ICL is mutagenic.

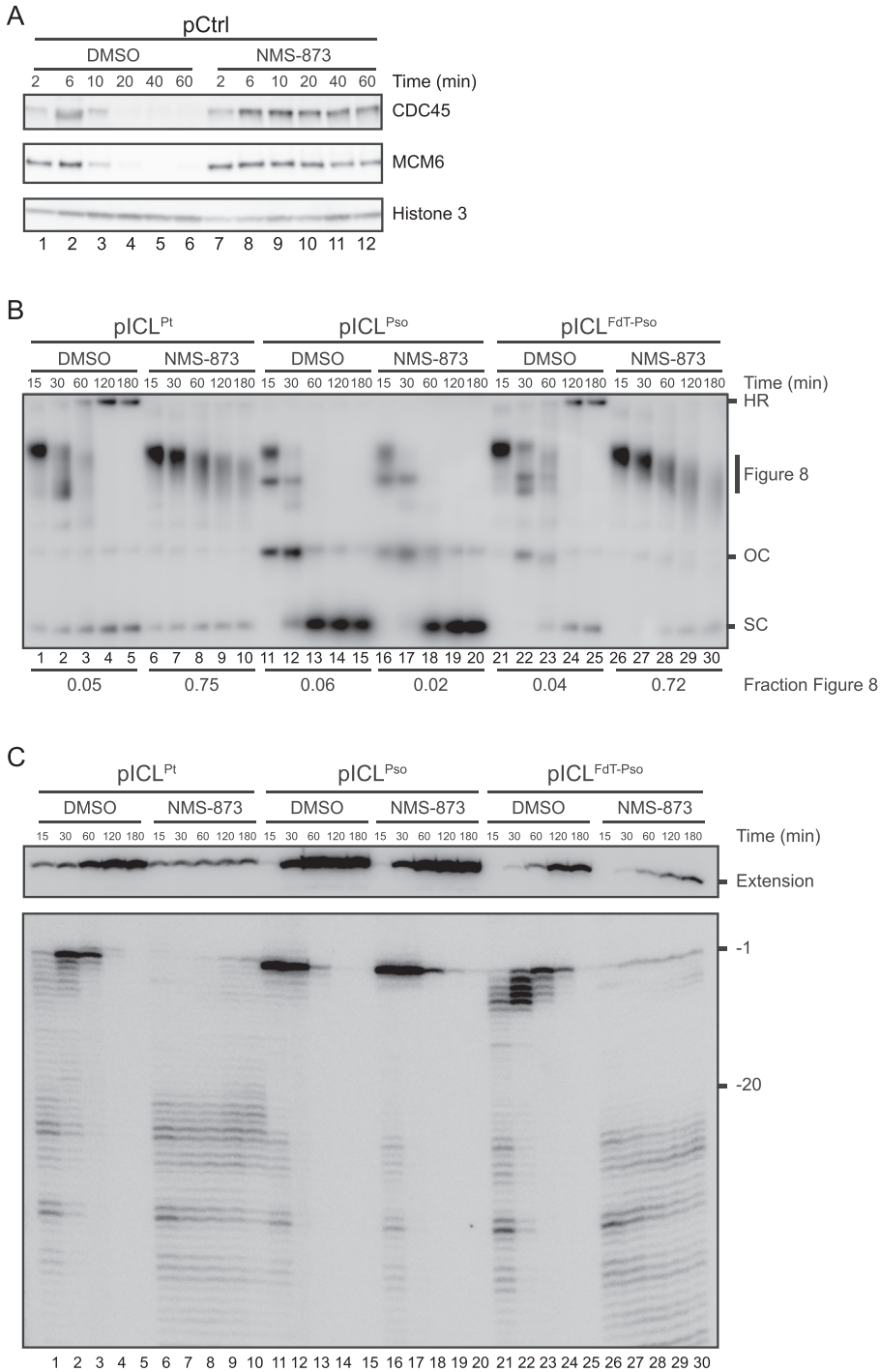

Figure S4. CMG Unloading Is Required for 2′FdT-Psoralen-ICL Repair, Related to Figure 4

(A) Plasmid pull down assays. pCtrl (containing 48 *lacO* repeats but without damage) was replicated in the presence or absence of the P97 inhibitor NMS-873, and samples were stopped at the indicated times, followed by plasmid pull down using LacI-coated beads. Western blotting was performed on chromatin samples with the indicated antibodies.

(B) pICL was replicated in the presence or absence of NMS-873 with [α-^{32}P]dATP and analyzed as in Figure 1C. The fraction Figure 8 indicates the proportion of Figure 8 structures relative to total species at 180 min.

(C) Samples from (B) were purified and digested with AflIII and EcoRI before separation on a denaturing polyacrylamide gel and visualization by autoradiography.

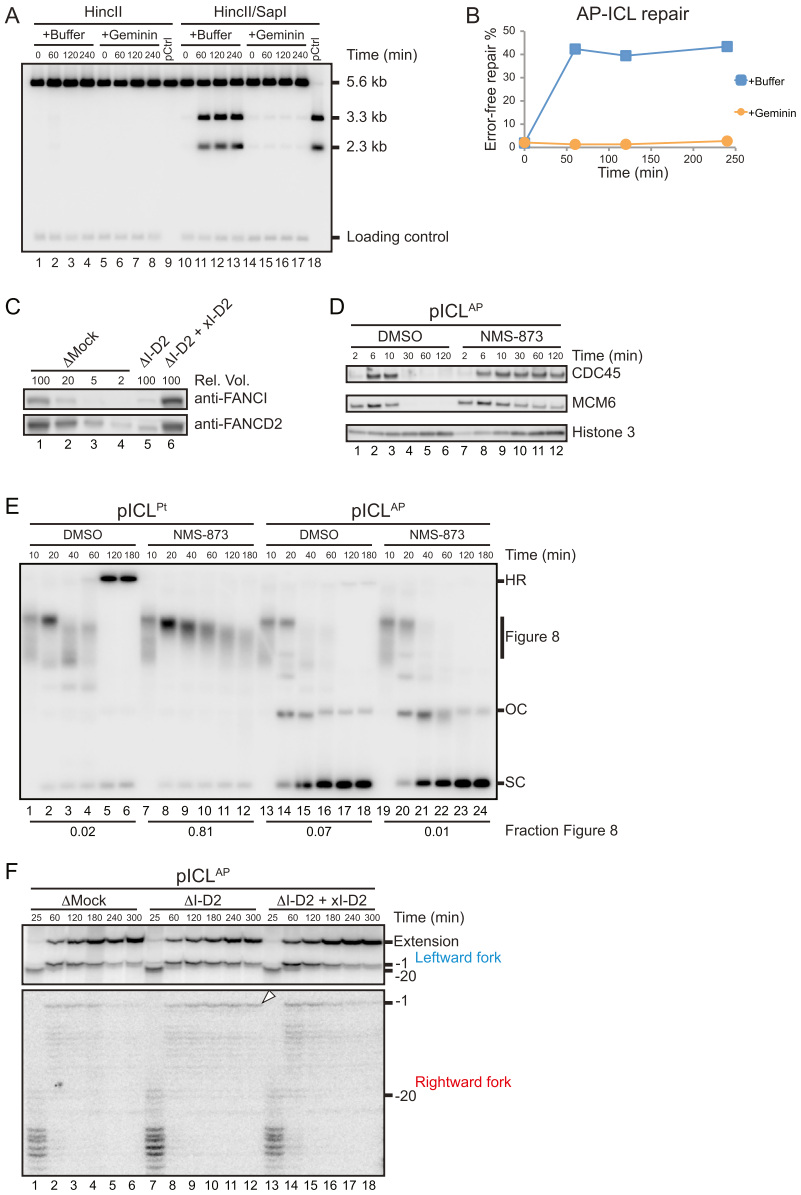

Figure S5. AP-ICL Repair Requires Replication, but Not CMG Unloading or FANCI-FANCD2, Related to Figure 5

(A) Error-free repair of pICL^{AP}. pICL^{AP} was replicated in egg extract in the presence or absence of geminin, as indicated. Repair intermediates were digested with HincII or HincII/SapI, separated on a native agarose gel, and visualized by Southern blotting. A 0.9 kb HindIII-digested pCtrl fragment was added before DNA extraction as a loading control. 50% of input pCtrl was digested with HincII or HincII/SapI and loaded in lanes 9 and 18, respectively. Digestion of repaired plasmids with HincII/SapI generates 3.3 kb and 2.3 kb fragments.

(B) Quantification of error-free repair efficiency of pICL^{AP} shown in (A). Efficiency of error-free pICL^{AP} repair was quantified as the ratio of error-free repair products to total linear species ([3.3 kb + 2.3 kb]/[5.6 kb +3.3 kb + 2.3 kb]) and graphed.

(C) FANCI-D2 immunodepletion. Mock-depleted and FANCI-D2-depleted NPE was analyzed by Western blotting using FANCI or FANCD2 antibody. A relative volume of 100 corresponds to 0.66 μl NPE.

(D) pICL^{AP} (containing 48 *lacO* repeats) was replicated in the presence or absence of NMS-873 and, at the indicated times, pulled down using LacI-coated beads. Chromatin samples were analyzed by Western blotting with the indicated antibodies.

(E) pICL^{Pt} and pICL^{AP} were replicated with [α-^{32}P]dATP in the presence or absence of NMS-873 and analyzed as in Figure 1C.

(F) pICL^{AP} was replicated in mock-depleted egg extract (ΔMock), FANCI-D2-depleted extract (ΔI-D2), or ΔI-D2 extract supplemented with xFANCI-D2 (ΔI-D2 + xI-D2) in the presence of [α-^{32}P]dATP. DNA was purified and digested with AflIII before separation on a denaturing polyacrylamide gel and visualization by autoradiography. Two portions of the autoradiograph are shown with different contrast for optimal display. White arrowhead, −1 product of the rightward fork that persists in the absence of FANCI-D2.

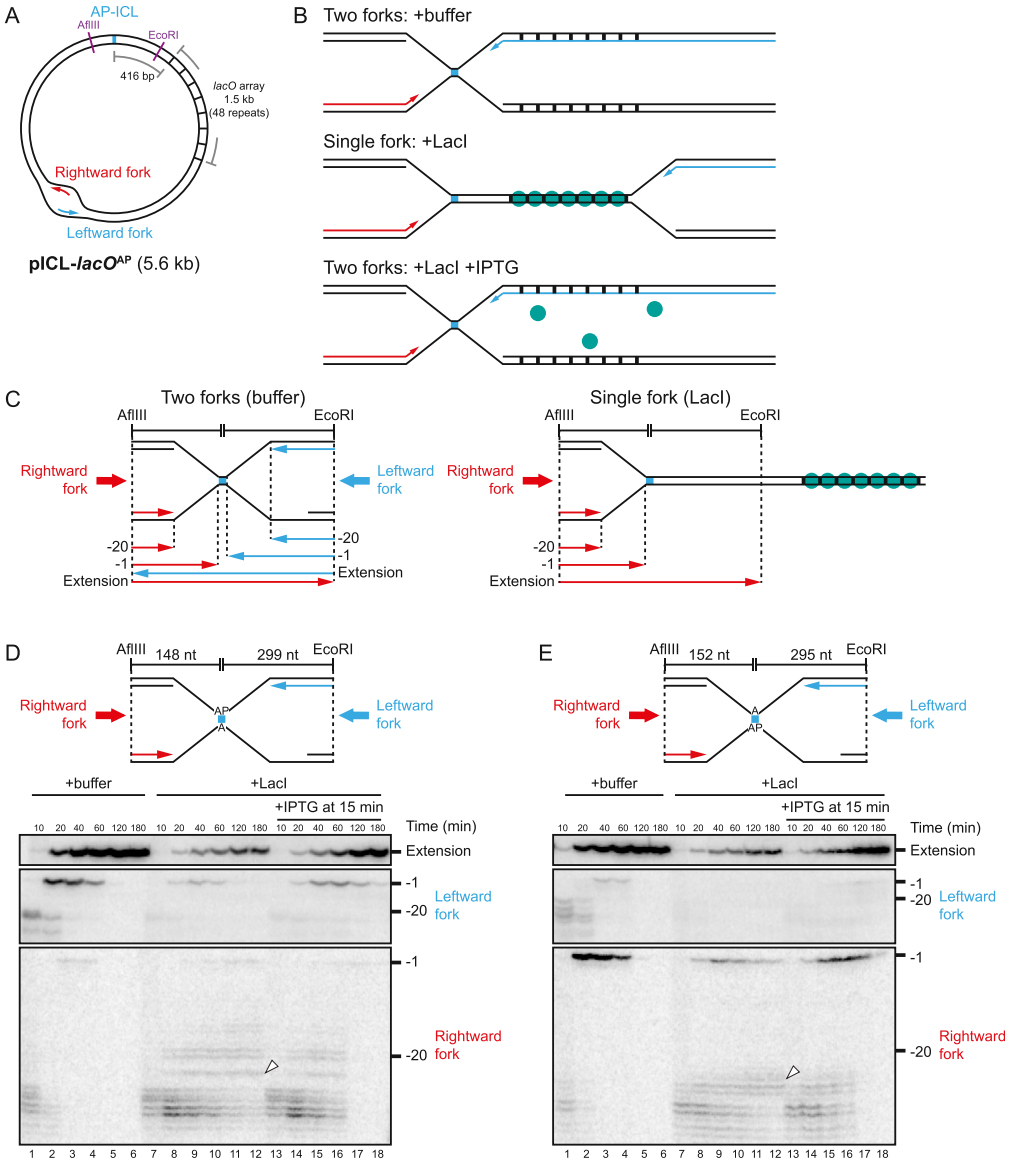

Figure S6. AP-ICL Unhooking Requires Replication Fork Convergence, Related to Figure 6

(A) Cartoon of pICL-*lacO*^{AP} containing an array of 48 *lacO* repeats. In order to determine whether AP-ICL repair requires convergence of two replication forks at the ICL (as seen for cisplatin- and psoralen-ICLs; Zhang et al., 2015), we constructed plasmids containing an AP-ICL adjacent to an array of 48 *lac* repressor binding sites. Binding of LacI to the *lacO* array prevents progression of the leftward replication fork to the ICL.

(B) Expected outcomes of pICL-*lacO*^{AP} replication in the presence of buffer, LacI, and LacI + IPTG. In the absence of LacI, two replication forks converge on the ICL. In the presence of LacI, progression of the leftward replication fork is blocked and only the rightward replication fork encounters the ICL. Addition of IPTG releases the block to leftward fork progression and both forks are able to converge on the ICL.

(C) Schematic illustration of nascent leading strands generated in the presence and absence of LacI in the experiments shown in (D) and (E).

(D and E) Nascent strand analysis of pICL-*lacO*^{AP} replication intermediates with the AP site on the top parental strand (D) or bottom parental strand (E), with or without LacI and IPTG, as indicated. pICL-*lacO*^{AP} plasmids were pre-incubated with buffer or LacI and then replicated in egg extract. At the times indicated, the nascent strands were purified, digested with AflIII and EcoRI, separated on a polyacrylamide gel, and visualized by autoradiography. Images were adjusted separately in different panels for optimal display. When the AP site is located on the top strand (and no LacI is present), prominent stalling of the leftward fork is observed (D, lanes 2-4), as in Figure 5F (lanes 14-16) due to a requirement for TLS to bypass the AP site. When the AP site is located on the bottom strand (and no LacI is present), prominent stalling of the rightward fork is seen (E, lanes 2-4). Importantly, when LacI is present to block arrival of the leftward fork, the AP-ICL causes persistent arrest of the rightward leading strand near the −20 position (arrowheads), regardless of whether the rightward leading strand encounters the adenosine-side (D) or the AP-side (E) of the ICL. Stalling at −20 is relieved by addition of IPTG, which causes LacI to dissociate form the *lacO* array and allows the leftward fork to encounter the ICL. This persistence of CMG at the AP-ICL (inferred from the −20 leading strand arrest) after arrival of only a single fork strongly implies that convergence of two replication forks is required to promote *N*-glycosyl bond cleavage.

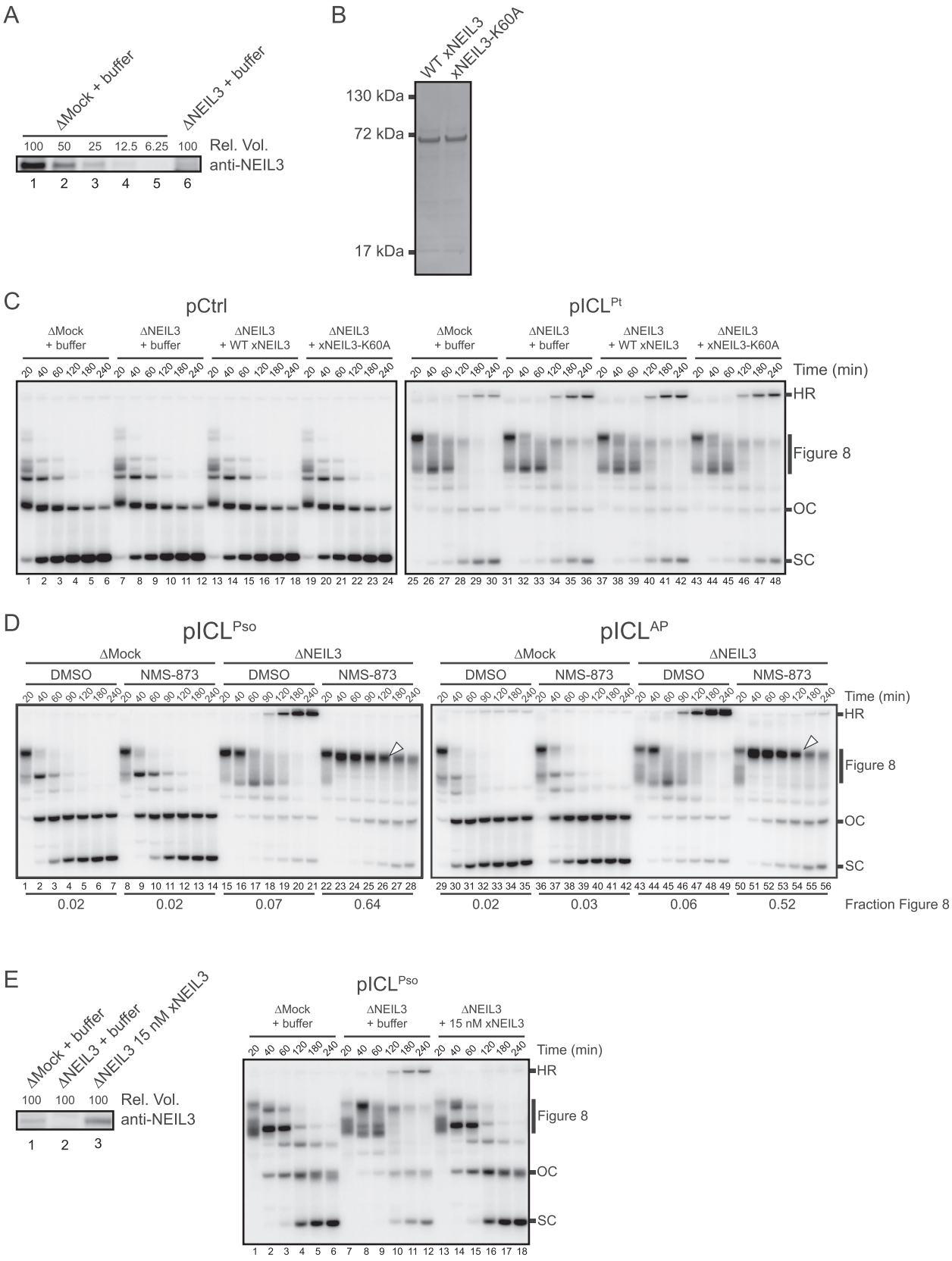

(legend on next page)

Figure S7. ICL Repair Requires CMG Unloading in the Absence of NEIL3-Dependent Unhooking, Related to Figure 7

(A) NEIL3 immunodepletion. Mock-depleted and NEIL3-depleted NPE was analyzed by Western blotting using NEIL3 antibody. A relative volume of 100 corresponds to 0.25 μl NPE.

(B) SDS-PAGE of recombinant NEIL3. Purified wild-type (WT) and K60A-mutated NEIL3 were separated on a 4%–20% acrylamide gel and visualized by Coomassie staining.

(C) pCtrl or pICL^{Pt} was replicated in mock-depleted egg extract, NEIL3-depleted egg extract, or NEIL3-depleted egg extract supplemented with recombinant NEIL3 in the presence of [α-^{32}P]dATP and analyzed as in Figure 1C.

(D) pICL^{Pso} or pICL^{AP} was replicated in mock-depleted or NEIL3-depleted egg extract supplemented with [α-^{32}P]dATP in the presence or absence of NMS-873 and analyzed as in Figure 1C. White arrowheads, Figure 8 structures that persist for pICL^{Pso} and pICL^{AP} in the presence of NMS-873 upon NEIL3-depletion. The fraction Figure 8 indicates the proportion of Figure 8 structures relative to total species at 240 min.

(E) 300 nM recombinant NEIL3 was used to rescue NEIL3 depletions in Figures 7A and S7C. However, we subsequently determined that the endogenous NEIL3 concentration is ~7 nM (left panel). We therefore repeated the rescue experiment and found that as little as ~15 nM recombinant NEIL3 was sufficient to rescue incision-independent unhooking in NEIL3-depleted extract (right panel). While 15 nM still exceeds the endogenous concentration by ~2-fold, this likely reflects the fact that recombinant NEIL3 is generally only partially active (Liu et al., 2012).